



MOX-Report No. 43/2019

**A space-time discontinuous Galerkin method for the
elastic wave equation**

Antonietti, P.F.; Mazzieri, I.; Migliorini, F.

MOX, Dipartimento di Matematica
Politecnico di Milano, Via Bonardi 9 - 20133 Milano (Italy)

mox-dmat@polimi.it

<http://mox.polimi.it>

A space-time discontinuous Galerkin method for the elastic wave equation

Paola F. Antonietti*, Ilario Mazzieri*, and Francesco Migliorini*

*MOX, Laboratory for Modeling and Scientific Computing, Dipartimento di Matematica, Politecnico di Milano, Piazza Leonardo da Vinci 32, I-20133 Milano, Italy
{paola.antonietti, ilario.mazzieri, francesco.migliorini}@polimi.it

October 21, 2019

Keywords : discontinuous Galerkin methods, wave equation, space-time finite elements, stability and convergence analysis.

Abstract

In this work we present a new high order space-time discretization method based on a discontinuous Galerkin paradigm for the second order visco-elastodynamics equation. After introducing the method, we show that the resulting space-time discontinuous Galerkin formulation is well-posed, stable and retains optimal rate of convergence with respect to the discretization parameters, namely the mesh size and the polynomial approximation degree. A set of three-dimensional numerical experiments confirms the theoretical bounds.

1 Introduction

Hyperbolic initial-boundary value problems, such as wave propagation phenomena, arise in many and different engineering disciplines: in sound and vibration analysis, in medical imaging, in sonar or radar detection, in computational seismology and in life and social sciences. Developing numerical methods for this class of problems has been a constant interest in the field of computational mechanics and engineering. To represent effectively the underlying physical phenomenon it is needed: i) an accurate representation of the waves propagating through the elastic or acoustic medium, ii) a detailed description of the involved geometry (such as complex surfaces and irregular interfaces) and iii) a considerable amount of computational effort in order to resolve the problem for all the wavelengths of interest.

Standard discretization methods in time and space are based on time-stepping methods (e.g. finite differences, Newmark or Runge-Kutta type schemes) combined with suitable spatial discretization techniques, like finite element methods. In this framework we can distinguish two families of methods: i) the method of lines, cf. [32] (first discretize in space and then solve the resulting ordinary differential equation) and ii) the Rothe method (first discretize in time and then solve the resulting partial differential equation), cf. [31].

More recently, discretizations of hyperbolic equations consider the full problem in the space-time configuration, i.e. the finite element method is also used to discretize the temporal

domain, and aim to overcome limitations of classical approaches such as issues of stability and convergence with the choice of parameters. Space-time finite element schemes can be divided in two classes according to which type of mesh they employ, i.e., an unstructured simplicial or a structured prismatic grid.

The first approach allows for discretization in time and space simultaneously because the temporal domain is treated as an additional dimension and a $d + 1$ -dimensional partition can be constructed directly in the space-time domain. In this sense, a one dimensional evolution problem is hence treated as a two dimensional one by considering, for instance, a triangular mesh. On the one hand, this approach has become quite popular and has been widely employed for problems that require deforming and/or moving meshes. See, for instance, [26, 12, 13, 29]. On the other hand, although recent advances in the generation of unstructured simplicial space-time meshes, see [43, 20], its construction for realistic three dimensional problems, hence composed of fourth dimensional polytopes, is still problematic and not easily achievable. It is mainly for that reason that space-time structured meshes are still preferable for three dimensional applications. Indeed, these grids can be easily obtained by extruding, in the time direction, the (generally) unstructured spatial mesh, giving rise to prismatic elements. The approximations built on top of such grids is less flexible than the one made by generic polytopes, but still allows for adaptivity. Additionally, the construction of space-time finite elements is very natural in this setting, [15, 41].

Looking only at time discretization, we can distinguish between time continuous space-time Galerkin method (TcG) and time-discontinuous Galerkin method (TdG). In TcG schemes no discontinuity in time is allowed in the approximation. In its general implementation, TcG involves high computational cost because the entire temporal domain has to be discretized. Relevant applications to the wave propagation problem can be found in [1, 44, 24, 34, 22, 33]. We refer the reader to [27, 28] for an exhaustive review on the subject.

In TdG schemes the time interval is further subdivided into independent time slabs and temporal discontinuities or jumps are allowed between the slabs. The finite element approach is applied in each time slab and the unknowns that are solved in one time slab serve as inputs for the following one. This formulation is much more efficient than the TcG one for obvious reasons. In particular, it has been shown that TdG scheme leads to approximations that are A-stable and high order accurate. In literature, it is possible to find different TdG finite element formulations that are built upon reformulating the original problem as a system of first-order equations (see, e.g., [19, 26, 30, 21]) or directly applied to the second-order hyperbolic system, where a Galerkin least square (GLS) approach is applied to stabilize the numerical scheme, e.g., [28, 42, 3, 45]).

In this paper we develop a new high-order *space-time* dG finite element method for the resolution of the visco-elastodynamics equation on prismatic grids. The scheme that we propose is the result of a combination between the *space* dG formulation introduced in [11] and the *time* dG approximation presented in [7]. In particular, for the spatial discretization is employed a combined dG-cG approach where the solution is allowed to be discontinuous subdomain-wise while it is continuous inside each subdomain and approximated with spectral elements, see e.g., [8, 36, 9]. For the time integration a recently introduced TdG method is applied to the second-order differential problem, [7] stemming after space discretization. The obtained TdG method is implicit and unconditionally stable, allowing independent displacement interpolations between different time slabs. This new space-time method is naturally

suitable for an adaptive choice of the time discretization parameters, i.e., the use of high-order polynomials/small time steps only when the solution features a sharp spatial-temporal derivative.

The remainder of the paper is organized as follows. In Section 2 we formulate the problem, we describe separately the space and time discretization techniques and their main properties. Then, we present the space-time dG method and we analyze its well-posedness. In Section 3 we derive the algebraic formulation while in Section 4 we investigate the stability of the scheme and we prove an *a-priori* error estimates. Finally, numerical results are shown in Section 5 concerning the verification and the validation of the proposed discretization. Throughout the paper, we use standard notation for Sobolev spaces [2]. The Sobolev spaces of vector-valued and symmetric tensor-valued functions are denoted by $\mathbf{H}^m(D) = [H^m(D)]^d$ and $\mathcal{H}^m(D) = [H^m(D)]_{\text{sym}}^{d \times d}$, respectively. We will use the symbol $(\cdot, \cdot)_D$ to denote the standard inner product in any of the spaces $\mathbf{H}^0(D) = \mathbf{L}^2(D)$ or $\mathcal{H}^0(D) = \mathcal{L}^2(D)$. For time dependent functions we define, for any $T > 0$, the spaces

$$L^q(0, T; H^s(\Omega)) = \{w : (0, T) \rightarrow H^s(\Omega) : \int_0^T \|w\|_{H^s(\Omega)}^q dt < +\infty, \quad 1 \leq q < \infty\},$$

and

$$H^q(0, T; H^s(\Omega)) = \{w : (0, T) \rightarrow H^s(\Omega) : \int_0^T \|w^{(k)}\|_{H^s(\Omega)}^2 dt < +\infty, \quad 1 \leq q < \infty, \quad 0 \leq k \leq q\},$$

for any $0 \leq s < \infty$. We define analogously the spaces $C^q(0, T; H^s(\Omega))$ for any $0 \leq q \leq \infty, 0 \leq s < \infty$ as well as the corresponding vector-valued counterparts. In the following C denotes a generic positive constant that may take different values in different places, but is always mesh (either in space and time) independent. The notation $x \lesssim y$ will represent the inequality $x \leq Cy$ for a constant C as before.

2 The visco-elastic wave propagation problem

We consider the general visco-elastic wave propagation problem in an open bounded polygonal domain $\Omega \subset \mathbb{R}^d$, $d = 2, 3$, with boundary $\partial\Omega = \Gamma_D \cup \Gamma_N$ such that $\Gamma_D \cap \Gamma_N = \emptyset$, and $|\Gamma_D| > 0$. The problem reads as follows: for $T > 0$ find $\mathbf{u} : \Omega \times (0, T] \rightarrow \mathbb{R}^d$ such that

$$\begin{cases} \rho \partial_{tt} \mathbf{u} + 2\rho\zeta \partial_t \mathbf{u} + \rho\zeta^2 \mathbf{u} - \nabla \cdot \boldsymbol{\sigma}(\mathbf{u}) = \mathbf{f}, & \text{in } \Omega \times (0, T], \\ \boldsymbol{\sigma}(\mathbf{u}) - \mathbf{D}\boldsymbol{\epsilon}(\mathbf{u}) = \mathbf{0}, & \text{in } \Omega \times (0, T], \\ \mathbf{u} = \mathbf{0}, & \text{on } \Gamma_D \times (0, T], \\ \boldsymbol{\sigma}(\mathbf{u})\mathbf{n} = \mathbf{0}, & \text{on } \Gamma_N \times (0, T], \\ \partial_t \mathbf{u}(0) = \hat{\mathbf{u}}_1(\mathbf{x}), & \text{in } \Omega \times \{0\}, \\ \mathbf{u}(0) = \hat{\mathbf{u}}_0(\mathbf{x}), & \text{in } \Omega \times \{0\}, \end{cases} \quad (1)$$

where $\rho \in L^\infty(\Omega)$ is a positive, bounded function representing the mass density of the medium, $\zeta \in L^\infty(\Omega)$ is a positive decay factor whose dimension is the inverse of time,

$\mathbf{f} \in C^1((0, T]; \mathbf{L}^2(\Omega))$ is a given source term, $\hat{\mathbf{u}}_0 \in \mathbf{H}_{0, \Gamma_D}^1(\Omega) \cap \mathbf{H}_D^\Delta(\Omega)$ and $\hat{\mathbf{u}}_1 \in \mathbf{H}_{0, \Gamma_D}^1(\Omega)$ are smooth enough initial conditions and

$$\begin{aligned} \mathbf{H}_{0, \Gamma_D}^1(\Omega) &= \{\mathbf{w} \in \mathbf{H}^1(\Omega) : \mathbf{w} = \mathbf{0} \text{ on } \Gamma_D\}, \\ \mathbf{H}_D^\Delta(\Omega) &= \{\mathbf{w} \in \mathbf{L}^2(\Omega) : \operatorname{div}(\mathbf{D}\boldsymbol{\epsilon}(\mathbf{w})) \in \mathbf{L}^2(\Omega)\}. \end{aligned}$$

We remark that the damping factor ζ has been introduced to model viscoelastic effects without resorting to constitutive laws based on Prony series, which involve time convolutions to express the stress in terms of the strain history (see e.g. [38, 39]). The main idea is to regard the sum of ζ -dependent terms as a viscous displacement-dependent volume force $\mathbf{f}_{vs} = -2\rho\zeta\partial_t\mathbf{u} - \rho\zeta^2\mathbf{u}$ acting upon a purely elastic body undergoing a displacement field \mathbf{u} (see e.g. [8]). It can be shown that, considering an harmonic excitation, the solution \mathbf{u} obtained by adding the viscous force can be related to the solution $\hat{\mathbf{u}}$ of the corresponding linear elastic problem by the relation $\mathbf{u} = e^{-\zeta t}\hat{\mathbf{u}}$. Hence, every frequency component of the solution to the linear elastic problem is attenuated by an exponential factor.

The second equation in (1) is the Hooke's constitutive law and relates the strain tensor $\boldsymbol{\epsilon}(\mathbf{u}) = \frac{1}{2}(\nabla\mathbf{u} + \nabla\mathbf{u}^T)$ to the stress tensor $\boldsymbol{\sigma}$ through the 4th order uniformly bounded symmetric and positive definite stiffness tensor \mathbf{D} defined as follows

$$\mathbf{D}\boldsymbol{\epsilon} = 2\mu\boldsymbol{\epsilon} + \lambda\operatorname{tr}(\boldsymbol{\epsilon})\mathbf{I}. \quad (2)$$

In (2), λ and μ are the first and second Lamé elastic coefficients, respectively, while $\operatorname{tr}(\cdot)$ is the trace operator and $\mathbf{I} \in \mathbb{R}^{d \times d}$ is the identity tensor. Hereafter, we suppose that λ and μ are uniformly bounded positive functions in Ω , i.e., $\lambda, \mu \in L^\infty(\Omega)$, $\lambda, \mu > 0$. Next, we consider the variational formulation of problem (1): for all $t \in (0, T]$ find $\mathbf{u} \in \mathbf{H}_{0, \Gamma_D}^1(\Omega)$ such that:

$$(\rho\mathbf{u}_{tt}, \mathbf{v})_\Omega + (2\rho\zeta\partial_t\mathbf{u}, \mathbf{v})_\Omega + (\rho\zeta^2\mathbf{u}, \mathbf{v})_\Omega + (\boldsymbol{\sigma}(\mathbf{u}), \boldsymbol{\epsilon}(\mathbf{v}))_\Omega = (\mathbf{f}, \mathbf{v})_\Omega \quad \forall \mathbf{v} \in \mathbf{H}_{0, \Gamma_D}^1(\Omega), \quad (3)$$

supplemented with the initial conditions $\mathbf{u}(0) = \hat{\mathbf{u}}_0$ and $\mathbf{u}_t(0) = \hat{\mathbf{u}}_1$. Under the above regularity assumptions problem (3) has a unique solution $\mathbf{u} \in C^2(0, T; \mathbf{L}^2(\Omega)) \cap C^1(0, T; \mathbf{H}_{0, \Gamma_D}^1(\Omega)) \cap C^0(0, T; \mathbf{H}_{0, \Gamma_D}^1(\Omega) \cap \mathbf{H}_D^\Delta(\Omega))$, see for instance [5, Theorem 3.1].

2.1 Space discretization based on a dG spectral element method

We consider a (not necessarily conforming) decomposition \mathcal{T}_h of Ω into L nonoverlapping polyhedral sub-domains Ω_ℓ , i.e., $\bar{\Omega} = \cup_\ell \bar{\Omega}_\ell$, $\Omega_\ell \cap \Omega_{\ell'} = \emptyset$ for $\ell \neq \ell'$. On each Ω_ℓ , we build a *conforming, quasi-uniform* computational mesh \mathcal{T}_{h_ℓ} of granularity $h_\ell > 0$ made by open disjoint elements \mathcal{K}_ℓ^j , and suppose that each $\mathcal{K}_\ell^j \in \Omega_\ell$ is the affine image through the map $F_\ell^j : \hat{\mathcal{K}} \rightarrow \mathcal{K}_\ell^j$ of either the unit reference hexahedron (resp. square) or the unit reference tetrahedron (resp. triangle) $\hat{\mathcal{K}}$ for $d = 3$ (resp. $d = 2$), see Fig. 1. Given two adjacent regions Ω_{ℓ^\pm} , we define an interior face F as the non-empty interior of $\partial\mathcal{K}^+ \cap \partial\mathcal{K}^-$, for some $\mathcal{K}^\pm \in \mathcal{T}_{h_{\ell^\pm}}$, $\mathcal{K}^\pm \subset \Omega_{\ell^\pm}$, and collect all the interior faces in the set \mathcal{F}_h^I . Moreover, we define \mathcal{F}_h^D and \mathcal{F}_h^N as the sets of all boundary faces where displacement and traction are imposed, respectively. Implicit in this definition is the assumption that each boundary face can belong to exactly one of the sets \mathcal{F}_h^D or \mathcal{F}_h^N . Finally, we collect all the boundary faces in the set \mathcal{F}_h^b . To carry out the analysis, we suppose that the following shape-regularity mesh assumption holds, see [37, 23].

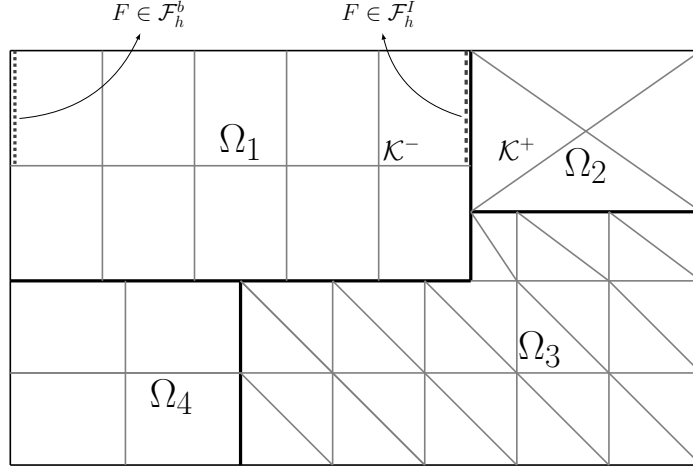


Figure 1: Two dimensional example of the domain decomposition partition. Non-conforming subdomain partition $\bar{\Omega} = \cup_{\ell} \bar{\Omega}_{\ell}$ and conforming quasi-uniform computational mesh within each Ω_{ℓ} .

Assumption 2.1. *Mesh assumption.* For any element $K \in \mathcal{T}_h$ and for any face $F \subset \partial K$, it holds $h_{\mathcal{K}} \lesssim h_F$.

Assumption 2.2. *Local bounded variation.* Mesh-size h_{ℓ} and polynomial degree N_{ℓ} have local bounded variation, i.e. $h_{\ell^+} \lesssim h_{\ell^-} \lesssim h_{\ell^+}$ and $N_{\ell^+} \lesssim N_{\ell^-} \lesssim N_{\ell^+}$ for any pair of neighboring elements $\Omega_{\ell^{\pm}}$,

We refer to [16], for example, for the weakening of the above assumptions and to [15, 6, 10] for the use of polyhedral-shaped elements.

Let $\mathcal{K}^{\pm} \in \mathcal{T}_{h_{\ell^{\pm}}}$ be two elements sharing a face $F \in \mathcal{F}_h^I$, and let \mathbf{n}^{\pm} be the unit normal vectors to F pointing outward to \mathcal{K}^{\pm} , respectively. For (regular enough) vector and tensor-valued functions \mathbf{w} and $\boldsymbol{\tau}$, respectively, we denote by \mathbf{w}^{\pm} and $\boldsymbol{\tau}^{\pm}$ the traces of \mathbf{w} and $\boldsymbol{\tau}$ on F , taken within the interior of \mathcal{K}^{\pm} , respectively, and set

$$[[\mathbf{w}]] = \mathbf{w}^+ \odot \mathbf{n}^+ + \mathbf{w}^- \odot \mathbf{n}^-, \quad [[\boldsymbol{\tau}]] = \boldsymbol{\tau}^+ \mathbf{n}^+ + \boldsymbol{\tau}^- \mathbf{n}^-, \quad \{\mathbf{w}\} = \frac{\mathbf{w}^+ + \mathbf{w}^-}{2}, \quad \{\boldsymbol{\tau}\} = \frac{\boldsymbol{\tau}^+ + \boldsymbol{\tau}^-}{2},$$

where $\mathbf{w} \odot \mathbf{n} = (\mathbf{w}^T \mathbf{n} + \mathbf{n}^T \mathbf{w})/2$.

Now, to each subdomain Ω_{ℓ} we assign a nonnegative integer N_{ℓ} , and introduce the finite dimensional spaces for $\ell = 1, \dots, L$,

$$\mathbf{V}_{h^{\ell}}^{N_{\ell}}(\Omega^{\ell}) = \{\mathbf{w} \in \mathbf{C}^0(\bar{\Omega}_{\ell}) : \mathbf{w}|_{\mathcal{K}_{\ell}^j} \circ F_{\ell}^j \in [\mathbb{M}^{N_{\ell}}(\hat{\mathcal{K}})]^d \quad \forall \mathcal{K}_{\ell}^j \in \mathcal{T}_{h_{\ell}}, \mathbf{w} = \mathbf{0} \text{ on } \Gamma_D\}, \quad (4)$$

where $\mathbb{M}^{N_k}(\hat{\mathcal{K}})$ is either the space $\mathbb{P}^{N_k}(\hat{\mathcal{K}})$ of polynomials of total degree at most N_k on $\hat{\mathcal{K}}$, if $\hat{\mathcal{K}}$ is the reference tetrahedron (resp. triangle), or the space $\mathbb{Q}^{N_k}(\hat{\mathcal{K}})$ of polynomials of degree N_k in each coordinate direction on $\hat{\mathcal{K}}$, if $\hat{\mathcal{K}}$ is the unit reference hexahedron (resp. square) in \mathbb{R}^3 (resp. \mathbb{R}^2). We then define the space \mathbf{V}_h^N as $\mathbf{V}_h^N = \prod_{\ell} \mathbf{V}_{h^{\ell}}^{N_{\ell}}(\Omega^{\ell})$. The semi-discrete dG spectral element approximation of problem (3) reads: $\forall t \in (0, T]$, find $\mathbf{u}_h = \mathbf{u}_h(t) \in \mathbf{V}_h^N$ such

that

$$\sum_{\ell=1}^L [(\rho\ddot{\mathbf{u}}_h, \mathbf{v})_{\Omega_\ell} + (2\rho\zeta\dot{\mathbf{u}}_h, \mathbf{v})_{\Omega_\ell} + (\rho\zeta^2\mathbf{u}_h, \mathbf{v})_{\Omega_\ell}] + \mathcal{B}_h(\mathbf{u}_h, \mathbf{v}) = \mathcal{F}_h(\mathbf{v}) \quad \forall \mathbf{v} \in \mathbf{V}_h^N, \quad (5)$$

subjected to the initial conditions $\mathbf{u}_h(0) = \hat{\mathbf{u}}_{0,h}$ and $\dot{\mathbf{u}}(0) = \hat{\mathbf{u}}_{1,h}$, where $\hat{\mathbf{u}}_{0,h}$ and $\hat{\mathbf{u}}_{1,h}$ are suitable approximation to $\hat{\mathbf{u}}_0$ and $\hat{\mathbf{u}}_1$, respectively. In (5) the right-hand side $\mathcal{F}_h(\cdot)$ is defined as

$$\mathcal{F}_h(\mathbf{v}) = \sum_{\ell=1}^L (\mathbf{f}, \mathbf{v})_{\Omega_\ell} \quad \mathbf{v} \in \mathbf{V}_h^N, \quad (6)$$

while the bilinear form $\mathcal{B}_h(\cdot, \cdot)$ is given by

$$\mathcal{B}_h(\mathbf{u}, \mathbf{v}) = \sum_{\ell=1}^L (\boldsymbol{\sigma}(\mathbf{u}), \boldsymbol{\epsilon}(\mathbf{v}))_{\Omega_\ell} - \langle \{\boldsymbol{\sigma}(\mathbf{u})\}, \llbracket \mathbf{v} \rrbracket \rangle_{\mathcal{F}_h^I} - \langle \llbracket \mathbf{u} \rrbracket, \{\boldsymbol{\sigma}(\mathbf{v})\} \rangle_{\mathcal{F}_h^I} + \langle \eta \llbracket \mathbf{u} \rrbracket, \llbracket \mathbf{v} \rrbracket \rangle_{\mathcal{F}_h^I}, \quad (7)$$

for any $\mathbf{u}, \mathbf{v} \in \mathbf{V}_h^N$ and where we have used the short-hand notation $\langle \mathbf{w}, \mathbf{v} \rangle_{\mathcal{F}_h^I} = \sum_{F \in \mathcal{F}_h^I} \langle \mathbf{w}, \mathbf{v} \rangle_F$.

In (7) the facewise stabilization function $\eta \in L^\infty(\mathcal{F}_h^I)$ is defined as

$$\eta|_F = \alpha \{\mathbf{D}\}_H \frac{\max\{N_{\ell+}^2, N_{\ell-}^2\}}{\min\{h_{\ell+}, h_{\ell-}\}}, \quad \forall F \in \mathcal{F}_h^I, \quad \bar{F} \subseteq \partial\bar{\Omega}_{\ell+} \cap \partial\bar{\Omega}_{\ell-}, \quad (8)$$

where α is a positive constant to be properly chosen and, for a piecewise constant tensor \mathbf{D} ,

$$\{\mathbf{D}\}_H = 2 \frac{((\mathbf{n}^+)^T \mathbf{D}^+ (\mathbf{n}^+)) ((\mathbf{n}^-)^T \mathbf{D}^- (\mathbf{n}^-))}{((\mathbf{n}^+)^T \mathbf{D}^+ (\mathbf{n}^+)) + ((\mathbf{n}^-)^T \mathbf{D}^- (\mathbf{n}^-))}.$$

Remark 2.3. If $L = 1$, i.e., if there is only one subdomain and $\mathcal{F}_h^I = \emptyset$, formulation (5) corresponds to the classical spectral element method, see e.g. [17, 18]. On the other hand, if Ω_ℓ for $\ell = 1, \dots, L$ consists of only one element, the dG paradigm is employed elementwise.

We next introduce the following (mesh-dependent) norms

$$\begin{aligned} \|\mathbf{w}\|_*^2 &= \sum_{\ell=1}^L \|\mathbf{D}^{1/2} \boldsymbol{\epsilon}(\mathbf{w})\|_{\mathcal{L}^2(\Omega_\ell)}^2 + \|\eta^{1/2} \llbracket \mathbf{w} \rrbracket\|_{\mathcal{L}^2(\mathcal{F}_h^I)}^2 \quad \forall \mathbf{w} \in \mathbf{H}^1(\mathcal{T}_\Omega), \\ \|\mathbf{w}\|_*^2 &= \|\mathbf{w}\|_*^2 + \|\eta^{-1/2} \{\mathbf{D} \boldsymbol{\epsilon}(\mathbf{w})\}\|_{\mathcal{L}^2(\mathcal{F}_h^I)}^2 \quad \forall \mathbf{w} \in \mathbf{H}^2(\mathcal{T}_\Omega), \end{aligned} \quad (9)$$

with the convention that $\|\mathbf{w}\|_{\mathbf{L}^2(\mathcal{F}_h^I)}^2 = \sum_{F \in \mathcal{F}_h^I} \|\mathbf{w}\|_{\mathbf{L}^2(F)}^2$. Using the trace-inverse inequalities [14, 40, 17] and Assumption 2.2, it can be proved that the norms $\|\cdot\|_*$ and $\|\llbracket \cdot \rrbracket\|_*$ are equivalent when restricted to the space \mathbf{V}_h^N . The well-posedness of the semi-discrete formulation (5) follows from the following result, cf. [4] for the proof.

Proposition 1. The bilinear form $\mathcal{B}_h(\cdot, \cdot) : \mathbf{V}_h^N \times \mathbf{V}_h^N \rightarrow \mathbb{R}$ defined as in (7) satisfies

$$|\mathcal{B}_h(\mathbf{w}, \mathbf{v})| \lesssim \|\mathbf{w}\|_* \|\mathbf{v}\|_*, \quad \mathcal{B}_h(\mathbf{v}, \mathbf{v}) \gtrsim \|\mathbf{v}\|_*^2 \quad \forall \mathbf{v}, \mathbf{w} \in \mathbf{V}_h^N,$$

where the second estimate holds provided that the parameter α appearing in the definition of the stabilization function (8) is chosen sufficiently large. Moreover,

$$|\mathcal{B}_h(\mathbf{w}, \mathbf{v})| \lesssim \|\llbracket \mathbf{w} \rrbracket\|_* \|\mathbf{v}\|_* \quad \forall \mathbf{w} \in \mathbf{H}^2(\mathcal{T}_h), \forall \mathbf{v} \in \mathbf{V}_h^N.$$

We now recall the stability and convergence properties of the semi-discrete solution to (5). We refer the reader to [8] for the detailed proofs. For any real $s \geq 0$, we denote by $\mathbf{H}^s(\mathcal{T}_\Omega)$ the space of piecewise \mathbf{H}^s vector-valued functions, we introduce the space-energy norm

$$\|\mathbf{w}\|_{\mathcal{E}}^2 = \|\sqrt{\rho}\dot{\mathbf{w}}\|_{\mathbf{L}^2(\Omega)}^2 + \|\sqrt{\rho}\zeta\mathbf{w}\|_{\mathbf{L}^2(\Omega)}^2 + \|\mathbf{w}\|_*^2 \quad \forall \mathbf{w} \in \mathbf{H}^1(\mathcal{T}_h). \quad (10)$$

and assess the following results.

Theorem 1. [8, Theorem 3.3] For any time $t \in (0, T]$, let $\mathbf{u}_h(t) \in \mathbf{V}_h^N$ be the solution of problem (5). If $\mathbf{f} \in L^2(0, T; \mathbf{L}^2(\Omega))$, then

$$\|\mathbf{u}_h(t)\|_{\mathcal{E}} \lesssim \|\mathbf{u}_h(0)\|_{\mathcal{E}} + \int_0^t \|\mathbf{f}(\tau)\|_{\mathbf{L}^2(\Omega)} d\tau, \quad 0 < t \leq T.$$

Theorem 2. [8, Theorem 3.6] Assume that, for any time $t \in (0, T]$, the solution $\mathbf{u}(t)$ of problem (1) together with its two first temporal derivatives satisfy $\mathbf{u}(t)|_{\Omega_\ell}$, $\dot{\mathbf{u}}(t)|_{\Omega_\ell}$, $\ddot{\mathbf{u}}(t)|_{\Omega_\ell} \in \mathbf{H}^{s_\ell}(\Omega_\ell)$, $\ell = 1, \dots, L$, $s_\ell \geq 2$. Let $\mathbf{u}_h(t)$ be the corresponding solution of the semi-discrete formulation (5) with a sufficiently large penalty parameter α in (8) and let $\mathbf{e}_h(t) = \mathbf{u}(t) - \mathbf{u}_h(t)$ for any $t \in (0, T]$. Then,

$$\sup_{t \in [0, T]} \|\mathbf{e}_h(t)\|_{\mathcal{E}}^2 \lesssim \sum_{\ell=1}^L \frac{h_\ell^{2\beta_\ell-2}}{N_\ell^{2s_\ell-3}} \left(\sup_{t \in [0, T]} \mathcal{I}(\mathbf{u})(t) + \int_0^T \mathcal{I}(\dot{\mathbf{u}})(\tau) d\tau \right), \quad \forall t \in (0, T],$$

where

$$\mathcal{I}(\mathbf{w}) = \|\dot{\mathbf{w}}\|_{\mathbf{H}^{s_\ell}(\Omega_\ell)}^2 + \|\mathbf{w}\|_{\mathbf{H}^{s_\ell}(\Omega_\ell)}^2$$

and $\beta_\ell = \min\{s_\ell, N_\ell + 1\}$, for all $\ell = 1, \dots, L$.

Now, we introduce the algebraic formulation of (5) that will be the starting point of the time discretization we will discuss in the next section. We denote by $N_{\text{dof}} = \dim(\mathbf{V}_h^N)$, by introducing a basis $\{\phi_i\}_{i=1}^{N_{\text{dof}}}$ for \mathbf{V}_h^N , we write

$$\mathbf{u}_h(\mathbf{x}, t) = \sum_{j=1}^{N_{\text{dof}}} U_j(t) \phi_j(\mathbf{x}), \quad (11)$$

where $U_j(t)$ are the expansion coefficients of $\mathbf{u}_h(t)$ in the chosen basis. By taking $\mathbf{v} = \phi_i$, $\forall i = 1, \dots, N_{\text{dof}}$, in (5) and using (11) we obtain the following system of second-order differential equations

$$M\ddot{\mathbf{U}}(t) + C\dot{\mathbf{U}}(t) + E\mathbf{U}(t) = \mathbf{F}(t), \quad (12)$$

with $\mathbf{U}(0) = \hat{\mathbf{U}}_0$ and $\dot{\mathbf{U}}(0) = \hat{\mathbf{U}}_1$, where $\mathbf{U}(t) \in \mathbb{R}^{N_{\text{dof}}}$ contains the expansion coefficients U_j in (11). The elements of the matrices M, C and E can be expressed as

$$M_{ij} = \sum_{\ell=1}^L (\rho \phi_j, \phi_i)_{\Omega_\ell}, \quad C_{ij} = \sum_{\ell=1}^L (2\rho\zeta \phi_j, \phi_i)_{\Omega_\ell}, \quad E_{ij} = \sum_{\ell=1}^L (\rho\zeta^2 \phi_j, \phi_i)_{\Omega_\ell} + \mathcal{B}_h(\phi_j, \phi_i), \quad (13)$$

for any $i, j = 1, \dots, N_{\text{dof}}$, while the right-hand side $F_i(t) = \mathcal{F}_h(\phi_i)$ for any $i = 1, \dots, N_{\text{dof}}$.

Remark 2.4. Problem (12) is well posed and admits a unique solution $\mathbf{U} \in \mathbf{H}^2(0, T]$ in the interval $(0, T]$, provided that $\mathbf{F} \in \mathbf{L}^2(0, T]$, see [35].

2.2 dG time discretization

In this section we briefly review the time integration scheme introduced in [7] that is used for the time integration of the system (12). Notice that the following approach is independent from the choice of finite element discretization applied to the general problem (1).

We consider a partition \mathcal{T}_k of the time interval $I = (0, T]$ made by N_T time-slabs such that $0 = t_0 < t_1 < \dots < t_n < \dots < t_{N_T} = T$ and define $I_n = (t_{n-1}, t_n]$ having length $k_n = t_n - t_{n-1}$, see Fig. 2. We define for (a regular enough function) \mathbf{w} , the time jump operator at t_n as

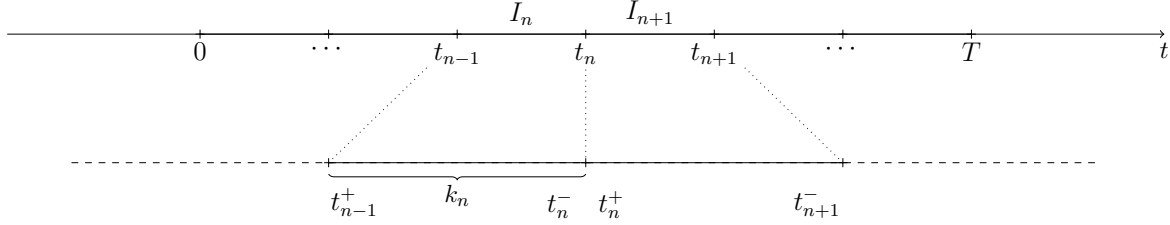


Figure 2: Example of time domain partition (top). Zoom of the time domain partition: values t_n^+ and t_n^- are also reported (bottom).

$$[\mathbf{w}]_n = \mathbf{w}(t_n^+) - \mathbf{w}(t_n^-), \quad \text{for } n \geq 0,$$

where

$$\mathbf{w}(t_n^\pm) = \lim_{\epsilon \rightarrow 0^\pm} \mathbf{w}(t_n + \epsilon), \quad \text{for } n \geq 0.$$

Moreover, we use the symbols $\mathbf{w}_n^+ = \mathbf{w}(t_n^+)$ and $\mathbf{w}_n^- = \mathbf{w}(t_n^-)$ to represent the trace of (a regular enough) \mathbf{w} , taken with the interior of I_{n+1} and I_n , respectively. Finally, we introduce the functional spaces

$$\mathbf{W}_{k_n}^{r_n} = \{\mathbf{w} : I_n \rightarrow \mathbb{R}^{N_{\text{dof}}} : \mathbf{w} \in [\mathbb{P}^{r_n}(I_n)]^{N_{\text{dof}}}\},$$

and

$$\mathbf{W}_k^r = \{\mathbf{w} \in \mathbf{L}^2(0, T) : \mathbf{w}|_{I_n} \in \mathbf{W}_{k_n}^{r_n} \forall n = 1, \dots, N_T\}.$$

Next, by multiplying equation (12) by a test function $\mathbf{V} \in \mathbf{W}_k^r$ and integrating it with respect to time we obtain the problem: find $\mathbf{U}_k \in \mathbf{W}_k^r$ such that

$$\begin{aligned} & \sum_{n=1}^{N_T} \left[(M\ddot{\mathbf{U}}_k, \dot{\mathbf{V}})_{I_n} + (C\dot{\mathbf{U}}_k, \dot{\mathbf{V}})_{I_n} + (E\mathbf{U}_k, \dot{\mathbf{V}})_{I_n} \right] + \sum_{n=1}^{N_T-1} \left[M[\dot{\mathbf{U}}_k]_n \cdot \dot{\mathbf{V}}(t_n^+) + E[\mathbf{U}_k]_n \cdot \mathbf{V}(t_n^+) \right] \\ & + M\dot{\mathbf{U}}_k(0^+) \cdot \dot{\mathbf{V}}(0^+) + E\mathbf{U}_k(0^+) \cdot \mathbf{V}(0^+) = \sum_{n=1}^{N_T} (\mathbf{F}, \dot{\mathbf{V}})_{I_n} + M\hat{\mathbf{U}}_1 \cdot \dot{\mathbf{V}}(0^+) + E\hat{\mathbf{U}}_0 \cdot \mathbf{V}(0^+), \end{aligned} \quad (14)$$

for any $\mathbf{V} \in \mathbf{W}_k^r$. Note that, thanks to the regularity assumption on \mathbf{U} , cf. Remark 2.4, we added to (12) the null terms $E[\mathbf{U}]_n$ and $[\dot{\mathbf{U}}]_n$ for any $n = 1, \dots, N_T$, see also [7]. Finally, we recall the following stability and convergence results of the time discretization (14). We refer

the reader to [7] for an exhaustive analysis of the method and for the complete proofs of the main results. We firstly introduce the energy norm

$$\begin{aligned} \|\mathbf{W}\|_E = & \sum_{n=1}^{N_T} \|C^{1/2}\dot{\mathbf{W}}\|_{\mathbf{L}^2(I_n)} + \frac{1}{2}(M^{1/2}\dot{\mathbf{W}}(0+))^2 + \frac{1}{2}\sum_{n=1}^{N_T} (M^{1/2}[\dot{\mathbf{W}}]_n)^2 + \frac{1}{2}(M^{1/2}\dot{\mathbf{W}}(T^-))^2 \\ & + \frac{1}{2}(E^{1/2}\mathbf{W}(0+))^2 + \frac{1}{2}\sum_{n=1}^{N_T} (E^{1/2}[\mathbf{W}]_n)^2 + \frac{1}{2}(E^{1/2}\mathbf{W}(T^-))^2, \end{aligned} \quad (15)$$

for any $\mathbf{W} \in \mathbf{W}_k^r$.

Theorem 3. [7, Proposition 3] Let $\mathbf{F} \in \mathbf{L}^2(0, T]$ and $\hat{\mathbf{U}}_0, \hat{\mathbf{U}}_1 \in \mathbb{R}^{N_{\text{dof}}}$. Then, the solution $\mathbf{U}_k \in \mathbf{W}_k^r$ of (14) satisfies

$$\|\mathbf{U}_k\|_E \lesssim \left(\|C^{1/2}\mathbf{F}\|_{\mathbf{L}^2(0, T)}^2 + (E^{1/2}\hat{\mathbf{U}}_0)^2 + (M^{1/2}\hat{\mathbf{U}}_1)^2 \right)^{\frac{1}{2}}.$$

Theorem 4. Let \mathbf{U} be the solution of (12) such that $\mathbf{U}|_{I_n} \in \mathbf{H}^{q_n}(I_n)$, for any $n = 1, \dots, N_T$ with $q_n \geq 2$, and let $\mathbf{U}_k \in \mathbf{W}_k^r$ be the solution of (14). Then, it holds

$$\|\mathbf{U} - \mathbf{U}_k\|_E^2 \lesssim \sum_{n=1}^{N_T} \frac{k_n^{2\beta_n-3}}{r_n^{2q_n-6}} \|\mathbf{U}\|_{\mathbf{H}^{q_n}(I_n)}, \quad (16)$$

where $\beta_n = \min\{r_n + 1, q_n\}$, for any $n = 1, \dots, N_T$, and the hidden constants depend on the infinity norm of the matrices M , C and E .

2.3 dG space-time discretization

In this section we present a space-time discontinuous Galerkin approximation that combine the discretization techniques described in Section 2.1 and Section 2.2. We consider a domain partition \mathcal{T} of the domain $Q = \Omega \times I$ obtained as the tensor product of space and time mesh grids, i.e, $\mathcal{T} = \mathcal{T}_h \otimes \mathcal{T}_k$. The general mesh element $Q_{\ell n} \in \mathcal{T}$ is a polytope of the form $Q_{\ell, n} = \mathcal{K}_\ell^j \otimes I_n$ where \mathcal{K}_ℓ^j is either a tetrahedron (resp. triangle) or a hexahedron (resp. square) in $\Omega_\ell \subset \mathcal{T}_h$ and I_n is the n -th time-slab. Notice that within this discretization we can allow for discontinuous approximation both in the space domain, i.e., across the hypersurface $\mathcal{F}_I \otimes I_n$ for $n = 1, \dots, N_T$, and in the time domain, i.e., along the interface $\mathcal{T}_h \otimes \{t_n\}$ for any $n = 1, \dots, N_T$. A sketch of a three dimensional (space-time) domain discretization is represented in Fig. 3.

The space-time dG finite element space $\mathcal{V}_{DG} = \mathbf{V}_h^N \otimes \mathbf{W}_k^r$ is defined based on the previous domain decomposition in the following way

$$\mathcal{V}_{DG} = \{\mathbf{w}(\mathbf{x}, t) = \mathbf{w}_1(\mathbf{x})w_2(t) : \mathcal{T}_h \times \mathcal{T}_k \rightarrow \mathbb{R}^3 : \mathbf{w}_1(\mathbf{x}) \in \mathbf{V}_h^N \text{ and } w_2(t) \in \mathbf{W}_k^r\}. \quad (17)$$

Now, we consider the first equation in (1) in the cylinder $Q_{\ell, n} = \Omega_\ell \otimes I_n$, we multiply it by a test function $\dot{\mathbf{v}}$, with $\mathbf{v} \in \mathcal{V}_{DG}$ and integrate in space and time over the cylinder $Q_{\ell, n}$, obtaining

$$(\rho\ddot{\mathbf{u}}, \dot{\mathbf{v}})_{Q_{\ell, n}} + (2\rho\zeta\dot{\mathbf{u}}, \dot{\mathbf{v}})_{Q_{\ell, n}} + (\rho\zeta^2\mathbf{u}, \dot{\mathbf{v}})_{Q_{\ell, n}} - (\nabla \cdot \boldsymbol{\sigma}(\mathbf{u}), \dot{\mathbf{v}})_{Q_{\ell, n}} = (\mathbf{f}, \dot{\mathbf{v}})_{Q_{\ell, n}}. \quad (18)$$

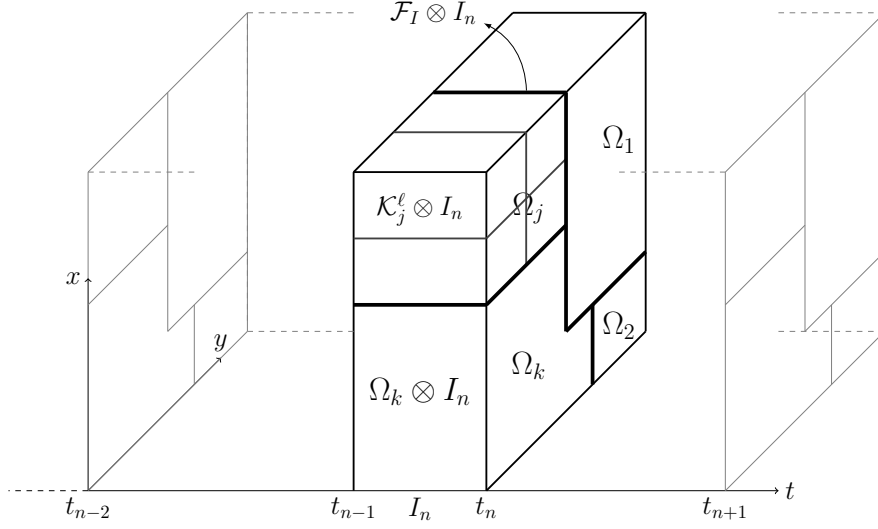


Figure 3: Example of space-time domain partition \mathcal{T} obtained as the tensor product of space and time mesh grids \mathcal{T}_h and \mathcal{T}_k , cf. Fig 1 and Fig 2, respectively. The general element mesh $\mathcal{K}_\ell^j \otimes I_n \in \mathcal{T}$ is also reported.

Next, being $\mathbf{u} \in C^1(0, T; \mathbf{L}^2(\Omega))$ we add the null terms

$$(\rho[\dot{\mathbf{u}}]_{n-1}, \dot{\mathbf{v}}(t_{n-1}^+))_\Omega, \quad (\rho\zeta^2[\mathbf{u}]_{n-1}, \mathbf{v}(t_{n-1}^+))_\Omega, \quad (\boldsymbol{\sigma}([\mathbf{u}]_{n-1}), \boldsymbol{\epsilon}(\mathbf{v}(t_{n-1}^+)))_\Omega, \quad (19)$$

we integrate by parts with respect to both space and time variables over $Q_{\ell n}$ and we sum up over all time slabs and all subdomains obtaining: find $\mathbf{u}_{DG} \in \mathcal{V}_{DG}$ such that

$$\mathcal{A}(\mathbf{u}_{DG}, \mathbf{v}) = \mathcal{F}(\mathbf{v}) \quad \forall \mathbf{v} \in \mathcal{V}_{DG}, \quad (20)$$

where

$$\begin{aligned} \mathcal{A}(\mathbf{w}, \mathbf{v}) &= \sum_{n=1}^{N_T} \sum_{\ell=1}^L [(\rho \mathbf{w}_1 \ddot{w}_2, \mathbf{v}_1 \dot{v}_2)_{Q_{\ell n}} + (2\rho\zeta \mathbf{w}_1 \dot{w}_2, \mathbf{v}_1 \dot{v}_2)_{Q_{\ell n}} + (\rho\zeta^2 \mathbf{w}_1 w_2, \mathbf{v}_1 \dot{v}_2)_{Q_{\ell n}}] \\ &+ \sum_{n=1}^{N_T} \mathcal{B}_h(\mathbf{w}_1, \mathbf{v}_1)(w_2, \dot{v}_2)_{I_n} + \sum_{n=1}^{N_T-1} \mathcal{B}_h(\mathbf{w}_1, \mathbf{v}_1)[w_2]_n v_2(t_n^+) + \mathcal{B}_h(\mathbf{w}_1, \mathbf{v}_1)w_2(0^+)v_2(0^+) \\ &+ \sum_{n=1}^{N_T-1} \sum_{\ell=1}^L [(\rho \mathbf{w}_1, \mathbf{v}_1)_{\Omega_\ell} [\dot{w}_2]_n \dot{v}_2(t_n^+) + (\rho\zeta^2 \mathbf{w}_1, \mathbf{v}_1)_{\Omega_\ell} [w_2]_n v_2(t_n^+)] \\ &+ \sum_{\ell=1}^L [(\rho \mathbf{w}_1, \mathbf{v}_1)_{\Omega_\ell} \dot{w}_2(0^+) \dot{v}_2(0^+) + (\rho\zeta^2 \mathbf{w}_1, \mathbf{v}_1)_{\Omega_\ell} w_2(0^+) v_2(0^+)], \end{aligned} \quad (21)$$

and

$$F(\mathbf{v}) = \sum_{n=1}^{N_T} \sum_{\ell=1}^L (\mathbf{f}, \mathbf{v}_1 \dot{v}_2)_{Q_{n\ell}} + \sum_{\ell=1}^L [(\rho \hat{\mathbf{u}}_1, \mathbf{v}_1)_{\Omega_\ell} \dot{v}_2(0^+) + (\rho\zeta^2 \hat{\mathbf{u}}_0, \mathbf{v}_1)_{\Omega_\ell} v_2(0^+)] + \mathcal{B}_h(\hat{\mathbf{u}}_0, \mathbf{v}_1) v_2(0^+), \quad (22)$$

for any $\mathbf{w}, \mathbf{v} \in \mathcal{V}_{DG}$.

In view of the forthcoming analysis we state the following result.

Proposition 2. *The function $||| \cdot ||| : H^2(0, T; \mathbf{H}_{0, \Gamma_D}^1(\Omega)) \rightarrow \mathbb{R}^+$ defined as*

$$|||\mathbf{w}|||^2 = \frac{1}{2} \|\mathbf{w}(0^+)\|_{\mathcal{E}}^2 + \frac{1}{2} \sum_{n=1}^{N_T-1} \|[\mathbf{w}]_n\|_{\mathcal{E}}^2 + \frac{1}{2} \|\mathbf{w}(T^-)\|_{\mathcal{E}}^2 + \sum_{n=1}^{N_T} \|\sqrt{2\rho\zeta}\dot{\mathbf{w}}\|_{\mathbf{L}^2(Q_n)}^2 \quad (23)$$

is a norm on $H^2(0, T; \mathbf{H}_{0, \Gamma_D}^1(\Omega))$.

Proof. It is clear that homogeneity and subadditivity hold, since $||| \cdot |||$ is the combination of norms. Therefore, we have only to show that $|||\mathbf{w}||| = 0 \iff \mathbf{w} = \mathbf{0} \forall \mathbf{w} \in H^2(0, T; \mathbf{H}_{0, \Gamma_D}^1(\Omega))$.

If $\mathbf{w} = \mathbf{0}$, it is immediate that $|||\mathbf{w}||| = 0$. Then, suppose that $|||\mathbf{w}||| = 0$. This implies that all the terms on the right hand side of (23) are null. Therefore, we have that

$$\|\sqrt{2\rho\zeta}\dot{\mathbf{w}}(t)\|_{\mathbf{L}^2(Q_n)}^2 = 0 \quad \forall n = 1, \dots, N_T,$$

that means $\partial_t \mathbf{w}(\mathbf{x}, t) = \mathbf{0}$ on each Q_n . In addition, from

$$\|\sqrt{\rho\zeta^2}\mathbf{w}(0^+)\|_{\mathbf{L}^2(\Omega)}^2 = 0,$$

we have that $\mathbf{w}(\mathbf{x}, 0^+) = \mathbf{0}$. It follows that \mathbf{w} satisfies

$$\begin{cases} \partial_t \mathbf{w}(\mathbf{x}, t) = \mathbf{0} & \text{on } Q_1, \\ \mathbf{w}(\mathbf{x}, 0^+) = \mathbf{0}, \end{cases}$$

and so $\mathbf{w} = \mathbf{0}$ on Q_1 . We proceed by induction and suppose $\mathbf{w}(\mathbf{x}, t) = \mathbf{0}$ on Q_{n-1} . Using that

$$\|\sqrt{\rho\zeta^2}[\mathbf{w}]_n\|_{\mathbf{L}^2(\Omega)}^2 = 0 \quad \forall n = 1, \dots, N_T - 1,$$

in (23), cf. also (10), and the induction assumption, we obtain

$$0 = [\mathbf{w}]_n = \mathbf{w}(\mathbf{x}, t_{n-1}^+) - \mathbf{w}(\mathbf{x}, t_{n-1}^-) = \mathbf{w}(\mathbf{x}, t_{n-1}^+)$$

Therefore, once again we have that

$$\begin{cases} \partial_t \mathbf{w}(\mathbf{x}, t) = \mathbf{0} & \text{on } Q_n, \\ \mathbf{w}(\mathbf{x}, t_{n-1}^+) = \mathbf{0}, \end{cases}$$

and so $\mathbf{w} = \mathbf{0}$ on $Q_n \forall n = 1, \dots, N_T - 1$. □

Remark 2.5. *If $\mathbf{w} \in \mathcal{V}_{DG}$ then we can write the energy norm (23) as*

$$\begin{aligned} |||\mathbf{w}|||^2 &= \mathcal{N}(\dot{w}_2) \|\sqrt{\rho}\mathbf{w}_1\|_{\mathbf{L}^2(\Omega)}^2 + \sum_{n=1}^{N_T} \|\dot{w}_2\|_{\mathbf{L}^2(I_n)}^2 \|\sqrt{2\rho\zeta}\mathbf{w}_1\|_{\mathbf{L}^2(\Omega)}^2 \\ &+ \mathcal{N}(w_2) \left[\|\sqrt{\rho\zeta^2}\mathbf{w}_1\|_{\mathbf{L}^2(\Omega)}^2 + \|\mathbf{w}\|_*^2 \right], \end{aligned} \quad (24)$$

where

$$\mathcal{N}(w) = \frac{1}{2} w(T^-)^2 + \frac{1}{2} w(0^+)^2 + \frac{1}{2} \sum_{n=1}^{N_T-1} ([w]_n)^2. \quad (25)$$

We are next ready to prove that (20) is well-posed.

Theorem 5. (Well-posedness). *Problem (20) admits a unique solution, provided that the stabilization parameter α in (8) is chosen large enough.*

Proof. We first show that $\mathcal{A}(\cdot, \cdot)$ is coercive w.r.t. the energy norm (10). Taking $\mathbf{u} = \mathbf{u}_1 u_2 \in \mathcal{V}_{DG}$, we have

$$\begin{aligned}
\mathcal{A}(\mathbf{u}, \mathbf{u}) &= \underbrace{\sum_{n=1}^{N_T} \sum_{\ell=1}^L [(\rho \mathbf{u}_1 \ddot{u}_2, \mathbf{u}_1 \dot{u}_2)_{Q_{\ell n}}]}_{T_1} + \underbrace{\sum_{n=1}^{N_T} \sum_{\ell=1}^L [(2\rho\zeta \mathbf{u}_1 \dot{u}_2, \mathbf{u}_1 \dot{u}_2)_{Q_{\ell n}}]}_{T_2} + \underbrace{\sum_{n=1}^{N_T} \sum_{\ell=1}^L [(\rho\zeta^2 \mathbf{u}_1 u_2, \mathbf{u}_1 \dot{u}_2)_{Q_{\ell n}}]}_{T_3} \\
&+ \underbrace{\sum_{n=1}^{N_T} \mathcal{B}_h(\mathbf{u}_1, \mathbf{u}_1)(u_2, \dot{u}_2)_{I_n}}_{T_4} + \underbrace{\sum_{n=1}^{N_T-1} \mathcal{B}_h(\mathbf{u}_1, \mathbf{u}_1)[u_2]_n u_2(t_n^+) + \mathcal{B}_h(\mathbf{u}_1, \mathbf{u}_1) u_2(0^+)^2}_{T_5} \\
&+ \underbrace{\sum_{n=1}^{N_T-1} \sum_{\ell=1}^L [(\rho \mathbf{u}_1, \mathbf{u}_1)_{\Omega_\ell} [\dot{u}_2]_n \dot{u}_2(t_n^+)]}_{T_7} + \underbrace{\sum_{n=1}^{N_T-1} \sum_{\ell=1}^L (\rho\zeta^2 \mathbf{u}_1, \mathbf{u}_1)_{\Omega_\ell} [u_2]_n u_2(t_n^+)}_{T_8} \\
&+ \underbrace{\sum_{\ell=1}^L (\rho \mathbf{u}_1, \mathbf{u}_1)_{\Omega_\ell} \dot{u}_2(0^+)^2}_{T_9} + \underbrace{(\rho\zeta^2 \mathbf{u}_1, \mathbf{u}_1)_{\Omega_\ell} u_2(0^+)^2}_{T_{10}}
\end{aligned}$$

Integrating by parts with respect to time the term T_1 we obtain

$$\begin{aligned}
\sum_{n=1}^{N_T} \sum_{\ell=1}^L (\rho \mathbf{u}_1 \ddot{u}_2, \mathbf{u}_1 \dot{u}_2)_{Q_{\ell n}} &= \sum_{\ell=1}^L \|\sqrt{\rho} \mathbf{u}_1\|_{\mathbf{L}^2(\Omega_\ell)}^2 \sum_{n=1}^{N_T} [-(\dot{u}_2, \ddot{u}_2)_{I_n} + \dot{u}_2(t_n^-)^2 - \dot{u}_2(t_{n-1}^+)^2] \\
&= \sum_{\ell=1}^L \|\sqrt{\rho} \mathbf{u}_1\|_{\mathbf{L}^2(\Omega_\ell)}^2 \sum_{n=1}^{N_T} \left[\frac{1}{2} \dot{u}_2(t_n^-)^2 - \frac{1}{2} \dot{u}_2(t_{n-1}^+)^2 \right],
\end{aligned}$$

and summing it up with T_7 and T_9 we have

$$T_1 + T_7 + T_9 = \sum_{\ell=1}^L \|\sqrt{\rho} \mathbf{u}_1\|_{\mathbf{L}^2(\Omega_\ell)}^2 \left[\frac{1}{2} \dot{u}_2(0^+)^2 + \frac{1}{2} \sum_{n=1}^{N_T-1} ([\dot{u}_2]_n^2 + \frac{1}{2} \dot{u}_2(T^-)^2) \right].$$

Then, we integrate by parts T_3 and sum it with T_8 and T_{10} obtaining

$$T_3 + T_8 + T_{10} = \sum_{\ell=1}^L \|\sqrt{\rho\zeta^2} \mathbf{u}_1\|_{\mathbf{L}^2(\Omega_\ell)}^2 \left[\frac{1}{2} u_2(0^+)^2 + \frac{1}{2} \sum_{n=1}^{N_T-1} ([u_2]_n^2 + \frac{1}{2} u_2(T^-)^2) \right],$$

and, similarly, for T_4 , T_5 and T_6 we obtain

$$\begin{aligned}
T_4 + T_5 + T_6 &= \sum_{n=1}^{N_T} \mathcal{B}_h(\mathbf{u}_1, \mathbf{u}_1)(u_2, \dot{u}_2)_{I_n} + \sum_{n=1}^{N_T-1} \mathcal{B}_h(\mathbf{u}_1, \mathbf{u}_1)[u_2]_n u_2(t_n^+) + \mathcal{B}_h(\mathbf{u}_1, \mathbf{u}_1) u_2(0^+)^2 \\
&= \mathcal{B}_h(\mathbf{u}_1, \mathbf{u}_1) \left[\frac{1}{2} u_2(0^+)^2 + \frac{1}{2} \sum_{n=1}^{N_T-1} [u_2]_n^2 + \frac{1}{2} u_2(T^-)^2 \right].
\end{aligned}$$

Now, using the coercivity of the bilinear form $\mathcal{B}_h(\cdot, \cdot)$, of Proposition 1, and definition (25), we obtain

$$\begin{aligned} \mathcal{A}(\mathbf{u}, \mathbf{u}) &\gtrsim \mathcal{N}(\dot{u}_2) \|\sqrt{\rho} \mathbf{u}_1\|_{\mathbf{L}^2(\Omega)}^2 + \sum_{n=1}^{N_T} \|\dot{u}_2\|_{L^2(I_n)}^2 \|\sqrt{2\rho\zeta} \mathbf{u}_1\|_{\mathbf{L}^2(\Omega)}^2 \\ &\quad + \mathcal{N}(u_2) \left[\|\sqrt{\rho\zeta^2} \mathbf{u}_1\|_{\mathbf{L}^2(\Omega)}^2 + \|\mathbf{u}_1\|_*^2 \right] = \|\mathbf{u}\|^2. \end{aligned}$$

We now prove the continuity of $\mathcal{F}(\cdot)$. Using definition (22), the arithmetic-geometric inequality and the Cauchy-Schwartz inequality we have that

$$\begin{aligned} |\mathcal{F}(\mathbf{v})|^2 &\lesssim \|(2\rho\zeta)^{-\frac{1}{2}} \mathbf{f}\|_{\mathbf{L}^2(Q)}^2 \|\sqrt{2\rho\zeta} \mathbf{v}_1\|_{\mathbf{L}^2(\Omega)}^2 \sum_{n=1}^{N_T} \|\dot{v}_2\|_{L^2(I_n)}^2 + \|\hat{\mathbf{u}}_1\|_{\mathbf{L}^2(\Omega)}^2 \|\sqrt{\rho} \mathbf{v}_1\|_{\mathbf{L}^2(\Omega)}^2 \dot{v}_2(0^+)^2 \\ &\quad + \left[\|\hat{\mathbf{u}}_0\|_{\mathbf{L}^2(\Omega)}^2 \|\sqrt{\rho\zeta^2} \mathbf{v}_1\|_{\mathbf{L}^2(\Omega)}^2 + \mathcal{B}_h(\hat{\mathbf{u}}_0, \mathbf{v}_1)^2 \right] \dot{v}_2(0^+)^2 \quad \forall \mathbf{v} = \mathbf{v}_1 \dot{v}_2 \in \mathcal{V}_{DG}. \end{aligned}$$

Now, using the continuity of $\mathcal{B}_h(\cdot, \cdot)$ in Proposition 1, i.e.,

$$|\mathcal{B}_h(\hat{\mathbf{u}}_0, \mathbf{v}_1)| \lesssim \|\hat{\mathbf{u}}_0\|_* \|\mathbf{v}_1\|_*$$

we can easily obtain

$$|\mathcal{F}(\mathbf{v})| \lesssim \left[\|(2\rho\zeta)^{-\frac{1}{2}} \mathbf{f}\|_{\mathbf{L}^2(Q)}^2 + \|\hat{\mathbf{u}}_1\|_{\mathbf{L}^2(\Omega)}^2 + \|\hat{\mathbf{u}}_0\|_{\mathbf{L}^2(\Omega)}^2 + \|\hat{\mathbf{u}}_0\|_* \right]^{\frac{1}{2}} \|\mathbf{v}\|,$$

and this concludes the proof. \square

As a direct consequence of the previous theorem we have the following result

Theorem 6. (*Stability*). *Let $\mathbf{u}_{DG} \in \mathcal{V}_{DG}$ be the solution of (20) and let $\mathbf{f} \in C^1((0, T]; \mathbf{L}^2(\Omega))$, $\hat{\mathbf{u}}_0 \in \mathbf{H}_{0, \Gamma_D}^1(\Omega) \cap \mathbf{H}_D^\Delta(\Omega)$ and $\hat{\mathbf{u}}_1 \in \mathbf{H}_{0, \Gamma_D}^1(\Omega)$. Then, it holds*

$$\|\|\mathbf{u}_{DG}\|\|^2 \lesssim \|(2\rho\zeta)^{-\frac{1}{2}} \mathbf{f}\|_{\mathbf{L}^2(Q)}^2 + \|\hat{\mathbf{u}}_1\|_{\mathbf{L}^2(\Omega)}^2 + \|\hat{\mathbf{u}}_0\|_{\mathbf{L}^2(\Omega)}^2 + \|\hat{\mathbf{u}}_0\|_*, \quad (26)$$

where the hidden constant is independent of the discretization parameters.

Proof. The proof follows from the coercivity of the bilinear form $\mathcal{A}(\cdot, \cdot)$ and the continuity of the linear functional $\mathcal{F}(\cdot)$. \square

3 Algebraic formulation

We derive here the algebraic formulation corresponding to problem (20) for the time slab I_n , $n = 1, \dots, N_T - 1$. Notice that the employment of discontinuous approximation between different hypersurfaces $\mathcal{T}_h \otimes \{t_n\}$ allows to compute the solution of the problem separately for one time slab at a time. Indeed, the weak formulation (20) restricted to I_n reads as: find $\mathbf{u}_{DG}^n \equiv \mathbf{u}_{DG}|_{I_n} \in V_h^N \times \mathbf{W}_{k_n}^{r_n}$ such that

$$\mathcal{A}_n(\mathbf{u}_{DG}^n, \mathbf{v}) = \mathcal{F}_n(\mathbf{v}) \quad \forall \mathbf{v} \in V_h^N \times \mathbf{W}_{k_n}^{r_n}, \quad (27)$$

where

$$\begin{aligned}
\mathcal{A}_n(\mathbf{w}, \mathbf{v}) &= \sum_{\ell=1}^L [(\rho\mathbf{w}_1, \mathbf{v}_1)_{\Omega_\ell}(\ddot{w}_2, \dot{v}_2)_{I_n} + (2\rho\zeta\mathbf{w}_1, \mathbf{u}_1)_{\Omega_\ell}(\dot{w}_2, \dot{v}_2)_{I_n} + (\rho\zeta^2\mathbf{w}_1, \mathbf{v}_1)_{\Omega_\ell}(w_2, \dot{v}_2)_{I_n}] \\
&\quad + \mathcal{B}_h(\mathbf{w}_1, \mathbf{v}_1)(w_2, \dot{v}_2)_{I_n} + \mathcal{B}_h(\mathbf{w}_1, \mathbf{v}_1)w_2(t_{n-1}^+)v_2(t_{n-1}^+) \\
&\quad + \sum_{\ell=1}^L [(\rho\mathbf{w}_1, \mathbf{v}_1)_{\Omega_\ell}\dot{w}_2(t_{n-1}^+)\dot{v}_2(t_{n-1}^+) + (\rho\zeta^2\mathbf{w}_1, \mathbf{v}_1)_{\Omega_\ell}w_2(t_{n-1}^+)v_2(t_{n-1}^+)],
\end{aligned} \tag{28}$$

for any $\mathbf{w}, \mathbf{v} \in V_h^N \times \mathbf{W}_{k_n}^{r_n}$ and

$$\begin{aligned}
F_n(\mathbf{v}) &= \sum_{\ell=1}^L (\mathbf{f}, \mathbf{v}_1 \dot{v}_2)_{Q_{\ell n}} + \sum_{\ell=1}^L [(\rho\dot{\mathbf{u}}(t_{n-1}^-), \mathbf{v}_1)_{\Omega_\ell} \dot{v}_2(t_{n-1}^+) + (\rho\zeta^2\mathbf{u}(t_{n-1}^-), \mathbf{v}_1)_{\Omega_\ell} v_2(t_{n-1}^+)] \\
&\quad + \mathcal{B}_h(\mathbf{u}(t_{n-1}^-), \mathbf{v}_1)v_2(t_{n-1}^+),
\end{aligned} \tag{29}$$

for any $\mathbf{v} \in V_h^N \times \mathbf{W}_{k_n}^{r_n}$. Notice that in (29) the values $\dot{\mathbf{u}}(t_{n-1}^-)$ and $\mathbf{u}(t_{n-1}^-)$ computed for I_{n-1} are used as initial conditions for the current slab. Notice also that, for the slab I_1 , we set $\dot{\mathbf{u}}_1(t_0^-) = \hat{\mathbf{u}}_1$ and $\mathbf{u}_1(t_0^-) = \hat{\mathbf{u}}_0$. Let us set a basis $\{\phi_i(\mathbf{x})\psi^\ell(t)\}$ for $V_h^N \times \mathbf{W}_{k_n}^{r_n}$, where $\{\phi_i(\mathbf{x})\}_{i=1}^{N_{\text{dof}}}$, resp. $\{\psi^\ell(t)\}_{\ell=1}^{r_n+1}$ is basis for V_h^N , resp. $\mathbf{W}_{k_n}^{r_n}$, and fix $D = N_{\text{dof}}(r_n + 1)$. Then, we can write the trial function \mathbf{u}_{DG} as a linear combination of the basis functions, i.e.,

$$\mathbf{u}_{DG}(\mathbf{x}, t) = \sum_{j=1}^{N_{\text{dof}}} \sum_{m=1}^{r_n+1} \alpha_j^m \phi_j(\mathbf{x}) \psi^m(t),$$

where $\alpha_j^m \in \mathbb{R}$ for $j = 1, \dots, N_{\text{dof}}$ and $m = 1, \dots, r_n + 1$. Next, we write equation (27) for any test function $\phi_i(\mathbf{x})\psi^\ell(t)$, $i = 1, \dots, N_{\text{dof}}$, $\ell = 1, \dots, r_n + 1$, obtaining the algebraic system

$$A_n \boldsymbol{\alpha}_n = \mathbf{F}_n, \tag{30}$$

where on the interval I_n , $A_n \in \mathbb{R}^{D \times D}$ is the associated local stiffness matrices, $\boldsymbol{\alpha}_n \in \mathbb{R}^D$ the solution vector and $\mathbf{F}_n \in \mathbb{R}^D$ corresponds to the data. We next investigate the structure of the matrix A_n by defining the following local matrices for $\ell, m = 1, \dots, r_n + 1$,

$$\begin{aligned}
N_1^{\ell m} &= (\ddot{\psi}^m, \dot{\psi}^\ell)_{I_n}, & N_2^{\ell m} &= (\dot{\psi}^m, \dot{\psi}^\ell)_{I_n}, & N_3^{\ell m} &= (\psi^m, \dot{\psi}^\ell)_{I_n}, \\
N_4^{\ell m} &= \dot{\psi}^m(t_{n-1}^+) \dot{\psi}^\ell(t_{n-1}^+), & N_5^{\ell m} &= \psi^m(t_{n-1}^+) \psi^\ell(t_{n-1}^+).
\end{aligned}$$

Then, by using equation (28) we can write

$$A_n = M \otimes (N_1 + N_4) + C \otimes N_2 + E \otimes (N_3 + N_5),$$

where M, C and E are defined in (13) and $A \otimes B$ denotes the Kronecher tensor product between the matrix A and the matrix B . On the other hand, the right-hand side \mathbf{F}_n can be expressed as $\mathbf{F}_n = [F_{1,1}, \dots, F_{1,r_n+1}, F_{2,1}, \dots, F_{2,r_n+1}, \dots, F_{N_{\text{dof}},1}, \dots, F_{N_{\text{dof}},r_n+1}]^T$, where

$$\begin{aligned}
F_{i,k} &= \sum_{\ell=1}^L (\mathbf{f}, \phi_i \dot{\psi}^k)_{Q_{\ell n}} + \sum_{\ell=1}^L [(\rho\dot{\mathbf{u}}_{DG}(t_{n-1}^-), \phi_i)_{\Omega_\ell} \dot{\psi}^k(t_{n-1}^+) + (\rho\zeta^2\mathbf{u}_{DG}(t_{n-1}^-), \phi_i)_{\Omega_\ell} \psi^k(t_{n-1}^+)] \\
&\quad + \mathcal{B}_h(\mathbf{u}_{DG}(t_{n-1}^-), \phi_i) \psi^k(t_{n-1}^+),
\end{aligned}$$

for any $i = 1, \dots, N_{\text{dof}}$ and $k = 1, \dots, r_n + 1$. We remark that the matrix A_n associated to the linear system (30) is skew symmetric and, in the general case, has to be built for any time slab I_n . However, if the time discretization parameter are fix, i.e., the time integration step $k_n = k$ and the polynomial degree $r_n = r$ for any $n = 1, \dots, N_T - 1$, then the matrix A_n can be stored and factorized once and for all, at the beginning of the temporal loop.

4 Convergence analysis

In this section we will prove a space-time a-priori error estimate in the energy norm (23). To this aim, we first prove the following result.

Proposition 3. *Let $\mathbf{w} \in \mathcal{V}_{DG}$ be the solution of (20) and let $\mathbf{W} \in \mathbf{W}_k^r$ be the solution of problem (14). Then, $\|\mathbf{w}\| \lesssim \|\mathbf{W}\|_E$, provided that α in (8) is chosen large enough.*

Proof. We write $\mathbf{w} \in \mathcal{V}_{DG}$ as $\mathbf{w}(\mathbf{x}, t) = \mathbf{w}_1(\mathbf{x})w_2(t)$ with $\mathbf{w}_1(\mathbf{x}) = \sum_{j=1}^{N_{\text{dof}}} W_j \phi_j(\mathbf{x})$, being $\{\phi_j\}$ a basis for \mathbf{V}_h^N and we set $\mathbf{W}(t) = [W_1, \dots, W_{N_{\text{dof}}}]^T w_2(t)$. Therefore, using the definition of energy norm $\|\cdot\|$ in (10) we can write

$$\|\mathbf{w}(0^+)\|_{\mathcal{E}} = \|\sqrt{\rho}\dot{\mathbf{w}}(0^+)\|_{\mathbf{L}^2(\Omega)}^2 + \|\sqrt{\rho}\zeta\mathbf{w}(0^+)\|_{\mathbf{L}^2(\Omega)}^2 + \|\mathbf{w}(0^+)\|_* = T_1 + T_2 + T_3.$$

In particular T_1 reduces to

$$\begin{aligned} T_1 &= \dot{w}_2(0^+)^2 \|\sqrt{\rho}\mathbf{w}_1\|_{\mathbf{L}^2(\Omega)}^2 = \dot{w}_2(0^+)^2 \sum_{i,j=1}^{N_{\text{dof}}} W_i W_j (\rho\phi_i, \phi_j)_{\Omega} \\ &= \sum_{i,j=1}^{N_{\text{dof}}} W_i \dot{w}_2(0^+) M_{ij} W_j \dot{w}_2(0^+) = (M^{1/2} \dot{\mathbf{W}}(0^+))^2, \end{aligned}$$

while for T_2 and T_3 we have

$$\begin{aligned} T_2 + T_3 &= \dot{w}_2(0^+)^2 \left[\|\sqrt{\rho\zeta^2}\mathbf{w}_1\|_{\mathbf{L}^2(\Omega)}^2 + \sum_{\ell=1}^L \|\mathbf{D}^{1/2}\epsilon(\mathbf{w}_1)\|_{\mathcal{L}^2(\Omega_{\ell})}^2 + \|\sqrt{\eta}[[\mathbf{w}_1]]\|_{\mathcal{L}^2(\mathcal{F}_h^I)}^2 \right] \\ &\lesssim \dot{w}_2(0^+)^2 \left[\|\sqrt{\rho\zeta^2}\mathbf{w}_1\|_{\mathbf{L}^2(\Omega)}^2 + \sum_{\ell=1}^L \|\mathbf{D}^{1/2}\epsilon(\mathbf{w}_1)\|_{\mathcal{L}^2(\Omega_{\ell})}^2 + \|\sqrt{\eta}[[\mathbf{w}_1]]\|_{\mathcal{L}^2(\mathcal{F}_h^I)}^2 \right. \\ &\quad \left. - 2(\{\boldsymbol{\sigma}(\mathbf{w}_1)\}, [[\mathbf{w}_1]])_{\mathcal{F}_h^I} \right] \\ &\lesssim \dot{w}_2(0^+)^2 \sum_{i,j=1}^{N_{\text{dof}}} W_i W_j \left[(\rho\zeta^2\phi_i, \phi_j)_{\Omega} + (\boldsymbol{\sigma}(\phi_i), \epsilon(\phi_j))_{\Omega} + (\eta[[\phi_i]], [[\phi_i]])_{\mathcal{F}_h^I} \right. \\ &\quad \left. - (\{\boldsymbol{\sigma}(\phi_i)\}, [[\phi_j]])_{\mathcal{F}_h^I} - ([[\phi_i]], \{\boldsymbol{\sigma}(\phi_j)\})_{\mathcal{F}_h^I} \right] \lesssim (E^{1/2}\mathbf{W}(0^+))^2. \end{aligned}$$

where in the last step we have used α big enough. Proceeding similarly for the remaining

terms in (10) we obtain

$$\begin{aligned}
|||\mathbf{w}|||^2 &\lesssim \frac{1}{2}(M^{1/2}\dot{\mathbf{W}}(0^+))^2 + \frac{1}{2}\sum_{n=1}^{N_T}(M^{1/2}[\dot{\mathbf{W}}]_n)^2 + \frac{1}{2}(M^{1/2}\dot{\mathbf{W}}(T^-))^2 + \sum_{n=1}^{N_T}\|C^{1/2}\dot{\mathbf{W}}\|_{\mathbf{L}^2(I_n)} \\
&\quad + \frac{1}{2}(E^{1/2}\mathbf{W}(0^+))^2 + \frac{1}{2}\sum_{n=1}^{N_T}(E^{1/2}[\mathbf{W}]_n)^2 + \frac{1}{2}(E^{1/2}\mathbf{W}(T^-))^2 \\
&= \|\mathbf{W}\|_E^2.
\end{aligned}$$

□

We are now ready to prove the following error estimate.

Theorem 7. *Assume that the exact solution of problem (1) satisfies $\mathbf{u} \in H^2(0, T; \mathbf{H}^{s_\ell}(\Omega_\ell))$, $\ell = 1, \dots, L$, $s_\ell \geq 2$ and that $\mathbf{f} \in H^{q_n}(0, T; \mathbf{L}^2(\Omega)) \forall n = 1, \dots, N_T$. Let \mathbf{u}_{DG} be the solution of the discrete DG formulation given in (20) with α sufficiently large. Then, it holds*

$$|||\mathbf{u} - \mathbf{u}_{DG}|||^2 \lesssim \sum_{n=1}^{N_T} \frac{k_n^{2\gamma_n-3}}{r_n^{2q_n-6}} \left[\|\mathbf{u}_h(0)\|_{\mathcal{E}}^2 + \|\mathbf{f}\|_{H^{q_n}(0, T; \mathbf{L}^2(\Omega))}^2 \right] + \sum_{\ell=1}^L \frac{h_\ell^{2\beta_\ell-2}}{N_\ell^{2s_\ell-3}} \|\mathbf{u}\|_{\mathbf{H}^2(0, T; H^{s_\ell}(\Omega_\ell))}^2$$

where $\gamma_n = \min\{r_n + 1, q_n\}$ and $\beta_\ell = \min\{N_\ell + 1, s_\ell\}$.

Proof. Supposing that $\mathbf{u}_h \in \mathbf{V}_h^N$ is the solution to the semidiscrete problem (5) we can split the error $\mathbf{e} = \mathbf{u} - \mathbf{u}_{DG}$ as the sum of two contributions $\mathbf{e}_h = \mathbf{u} - \mathbf{u}_h$ and $\mathbf{e}_k = \mathbf{u}_h - \mathbf{u}_{DG}$, being the former the error due to space discretization while the latter the one obtain after time integration. Then, by triangle inequality we have

$$|||\mathbf{u} - \mathbf{u}_{DG}|||^2 \leq |||\mathbf{e}_h|||^2 + |||\mathbf{e}_k|||^2.$$

We first focus on $|||\mathbf{e}_h|||$. Since $\mathbf{e}_h \in H^2(0, T; \mathbf{H}^2(\Omega))$, it holds $[\dot{\mathbf{e}}_h]_n = [\mathbf{e}_h]_n = 0 \forall n = 1, \dots, N_T$ and then $|||\mathbf{e}_h|||$ reduces to

$$\begin{aligned}
|||\mathbf{e}_h|||^2 &= \frac{1}{2}\|\sqrt{\rho}\dot{\mathbf{e}}_h(T^-)\|_{\mathbf{L}^2(\Omega)}^2 + \frac{1}{2}\|\sqrt{\rho}\dot{\mathbf{e}}_h(0^+)\|_{\mathbf{L}^2(\Omega)}^2 + \sum_{n=1}^{N_T}\|\sqrt{2\rho\zeta}\dot{\mathbf{e}}_h\|_{\mathbf{L}^2(Q_n)}^2 \\
&\quad + \frac{1}{2}\|\sqrt{\rho\zeta^2}\mathbf{e}_h(T^-)\|_{\mathbf{L}^2(\Omega)}^2 + \frac{1}{2}\|\sqrt{\rho\zeta^2}\mathbf{e}_h(0^+)\|_{\mathbf{L}^2(\Omega)}^2 \\
&\quad + \frac{1}{2}\sum_{\ell=1}^L\|\mathbf{D}^{1/2}\boldsymbol{\epsilon}(\mathbf{e}_h(T^-))\|_{\mathcal{L}^2(\Omega_\ell)}^2 + \frac{1}{2}\sum_{\ell=1}^L\|\mathbf{D}^{1/2}\boldsymbol{\epsilon}(\mathbf{e}_h(0^+))\|_{\mathcal{L}^2(\Omega_\ell)}^2 \\
&\quad + \frac{1}{2}\|\sqrt{\eta}[\mathbf{e}_h(T^-)]\|_{\mathcal{L}^2(\mathcal{F}_h^I)}^2 + \frac{1}{2}\|\sqrt{\eta}[\mathbf{e}_h(0^+)]\|_{\mathcal{L}^2(\mathcal{F}_h^I)}^2.
\end{aligned}$$

By using the classical trace inequality, cf. [40], we get

$$\begin{aligned}
|||\mathbf{e}_h|||^2 &\lesssim \int_0^T \left[\|\sqrt{\rho}\dot{\mathbf{e}}_h\|_{\mathbf{L}^2(\Omega)}^2 + \|\sqrt{\rho\zeta^2}\mathbf{e}_h\|_{\mathbf{L}^2(\Omega)}^2 + \sum_{\ell=1}^L \|\mathbf{D}^{1/2}\boldsymbol{\epsilon}(\mathbf{e}_h)\|_{\mathcal{L}^2(\Omega_\ell)}^2 + \|\sqrt{\eta}[\mathbf{e}_h]\|_{\mathcal{L}^2(\mathcal{L}_h^I)}^2 \right] + \\
&\quad + \int_0^T \left[\|\sqrt{\rho}\ddot{\mathbf{e}}_h\|_{\mathbf{L}^2(\Omega)}^2 + \|\sqrt{\rho\zeta^2}\dot{\mathbf{e}}_h\|_{\mathbf{L}^2(\Omega)}^2 + \sum_{\ell=1}^L \|\mathbf{D}^{1/2}\boldsymbol{\epsilon}(\dot{\mathbf{e}}_h)\|_{\mathcal{L}^2(\Omega_\ell)}^2 + \|\sqrt{\eta}[\dot{\mathbf{e}}_h]\|_{\mathcal{L}^2(\mathcal{F}_h^I)}^2 \right] = \\
&= \int_0^T \|\mathbf{e}_h\|_{\mathcal{E}}^2 + \int_0^T \|\dot{\mathbf{e}}_h\|_{\mathcal{E}}^2.
\end{aligned}$$

We next use the result of Theorem 2 so that

$$\begin{aligned}\int_0^T \|\mathbf{e}_h\|_{\mathcal{E}}^2 &\lesssim \sum_{\ell=1}^L \frac{h_\ell^{2\beta_\ell-2}}{N_\ell^{2s_\ell-3}} \left(\int_0^T \mathcal{I}(\mathbf{u})(t) dt + T \int_0^T \mathcal{I}(\dot{\mathbf{u}})(t) dt \right) \\ \int_0^T \|\dot{\mathbf{e}}_h\|_{\mathcal{E}}^2 &\lesssim \sum_{\ell=1}^L \frac{h_\ell^{2\beta_\ell-2}}{N_\ell^{2s_\ell-3}} \left(\int_0^T \mathcal{I}(\dot{\mathbf{u}})(t) dt \right).\end{aligned}$$

with $\beta_\ell = \min\{s_\ell, N_\ell + 1\}$, for all $\ell = 1, \dots, L$ and the following inequalities

$$\begin{aligned}\int_0^T \mathcal{I}(\mathbf{u})(t) dt &= \int_0^T \left(\|\dot{\mathbf{u}}(t)\|_{\mathbf{H}^{s_\ell}(\Omega_\ell)}^2 + \|\mathbf{u}(t)\|_{\mathbf{H}^{s_\ell}(\Omega_\ell)}^2 \right) dt \leq \|\mathbf{u}\|_{H^2(0,T;\mathbf{H}^{s_\ell}(\Omega_\ell))}^2 \\ \int_0^T \mathcal{I}(\dot{\mathbf{u}})(t) dt &= \int_0^T \left(\|\ddot{\mathbf{u}}(t)\|_{\mathbf{H}^{s_\ell}(\Omega_\ell)}^2 + \|\dot{\mathbf{u}}(t)\|_{\mathbf{H}^{s_\ell}(\Omega_\ell)}^2 \right) dt \leq \|\mathbf{u}\|_{H^2(0,T;\mathbf{H}^{s_\ell}(\Omega_\ell))}^2,\end{aligned}$$

to obtain

$$\|\|\mathbf{e}_h\|\|^2 \lesssim \sum_{\ell=1}^L \frac{h_\ell^{2\beta_\ell-2}}{N_\ell^{2s_\ell-3}} \|\mathbf{u}\|_{H^2(0,T;\mathbf{H}^{s_\ell}(\Omega_\ell))}^2. \quad (31)$$

Now we estimate $\|\|\mathbf{e}_k\|\|$. By using the result in Proposition 3 and Theorem 4 we obtain

$$\begin{aligned}\|\|\mathbf{e}_k\|\| &\lesssim \|\mathbf{E}_k\|_E^2 \lesssim \sum_{n=1}^{N_T} \frac{k_n^{2\beta_n-3}}{r_n^{2q_n-6}} \|\mathbf{u}_h\|_{\mathbf{H}^{q_n}(I_n)}^2 \\ &\lesssim \sum_{n=1}^{N_T} \frac{k_n^{2\beta_n-3}}{r_n^{2q_n-6}} \int_{I_n} \left(\|\mathbf{u}_h(t)\|_{\mathbf{L}^2(\Omega)}^2 + \|\dot{\mathbf{u}}_h(t)\|_{\mathbf{L}^2(\Omega)}^2 + \dots + \|\mathbf{u}_h^{(q_n)}(t)\|_{\mathbf{L}^2(\Omega)}^2 \right) dt.\end{aligned}$$

where $\beta_n = \min\{r_n + 1, q_n\}$, for any $n = 1, \dots, N_T$. Finally, using the result of Theorem 1 we get

$$\int_{I_n} \|\mathbf{u}_h(t)\|_{\mathbf{L}^2(\Omega)}^2 dt \lesssim \int_{I_n} \|\mathbf{u}_h(t)\|_{\mathcal{E}}^2 dt \lesssim T \left(\|\mathbf{u}_h(0)\|_{\mathcal{E}}^2 + \int_0^T \|\mathbf{f}(\tau)\|_{\mathbf{L}^2(\Omega)}^2 d\tau \right),$$

and

$$\int_{I_n} \|\mathbf{u}_h^{(q_n)}\|_{\mathbf{L}^2(\Omega)}^2 \lesssim \int_{I_n} \|\mathbf{u}_h^{(q_n)}\|_{\mathcal{E}}^2 \lesssim T \left(\int_0^T \|\mathbf{f}^{(q_n)}(\tau)\|_{\mathbf{L}^2(\Omega)}^2 d\tau \right).$$

Then

$$\|\|\mathbf{e}_k\|\|^2 \lesssim \sum_{n=1}^{N_T} \frac{k_n^{2\beta_n-3}}{r_n^{2q_n-6}} \left(\|\mathbf{u}_h(0)\|_{\mathcal{E}}^2 + \|\mathbf{f}\|_{H^{q_n}(0,T;\mathbf{L}^2(\Omega))}^2 \right). \quad (32)$$

with $\beta_n = \min\{r_n + 1, q_n\}$. Putting together estimate (31) and (32) we obtain the thesis. \square

Corollary 4.1. *Under the same assumption of Theorem 7, suppose moreover that the solution to problem (1) is regular enough with $s_\ell = s \forall \ell = 1, \dots, L$ and $q_n = q \forall n = 1, \dots, N_T$. If we set $h_\ell = h$, $N_\ell = N \forall \ell = 1, \dots, L$ and $k_n = k$, $r_\ell = r \forall n = 1, \dots, N_T$, then it holds*

$$\|\|\mathbf{u} - \mathbf{u}_{DG}\|\| \lesssim \frac{k^{\gamma-3/2}}{r^{q-3}} \left[\|\mathbf{u}_h(0)\|_{\mathcal{E}} + \|\mathbf{f}\|_{H^q(0,T;\mathbf{L}(\Omega))} \right] + \frac{h^{\beta-1}}{N^{s-3/2}} \|\mathbf{u}\|_{\mathbf{H}^2(0,T;\mathbf{H}^s(\Omega_\ell))}^2, \quad (33)$$

where $\gamma = \min\{r + 1, q\}$ and $\beta = \min\{N + 1, s\}$.

5 Numerical results

In this section we present a set of numerical experiments to verify the theoretical bounds. The numerical results have been obtained with the open-source software SPEED (<http://speed.mox.polimi.it/>), see [36].

5.1 Verification test

We set $I = (0, T]$, $T = 10$, and $\Omega = (0, 1)^3$ with homogeneous Dirichlet boundary conditions, i.e. $\Gamma_N = 0$, $\Gamma_D = \partial\Omega$. We set the external force \mathbf{f} and the initial conditions \mathbf{u}_0 , \mathbf{u}_1 so that the exact solution of (1) is

$$\mathbf{u}(t) = \cos(3\pi t) \begin{bmatrix} \sin(\pi x)^2 \sin(2\pi y) \sin(2\pi z) \\ \sin(2\pi x) \sin(\pi y)^2 \sin(2\pi z) \\ \sin(2\pi x) \sin(2\pi y) \sin(\pi z)^2 \end{bmatrix}, \quad t \in [0, T]. \quad (34)$$

On the one hand, we consider a decomposition \mathcal{T}_h of Ω made by a single macro element, i.e. $\Omega = \Omega_1$, we introduce a conforming hexahedral mesh of granularity h in Ω_1 , and choose a polynomial degree $N_1 = N \geq 2$ for the spatial discretization. On the other hand, we use a uniform time domain partition of step size Δt and set a polynomial degree $r \geq 2$ for the temporal discretization. We compute the error $\|\mathbf{u}_{DG} - \mathbf{u}\|$ by employing the energy norm (23), and verify the error estimate (33) separately in space and time. We firstly set $h = 0.0125$ corresponding to 512 elements and fix $N = 4$, and let the time step Δt varying from 0.4 to 0.00625 for $r = 2, 3, 4$. The computed energy errors are shown in Figure 4. We can observe that the numerical results are in agreement with the theoretical ones. We note that with $r = 4$, the error reaches a plateau for $\Delta t \leq 0.025$. However, this effect could be easily overcome by increasing the spatial polynomial degree N and/or by refining the mesh size h .

Now, we fix the time step $\Delta t = 0.001$, the polynomial degree $r = 5$ and we use increasingly refined spatial grids with $h = 0.5, 0.25, 0.2, 0.125, 0.0625$, for different choices of the polynomial degree $N = 2, 3, 4$. The results are shown in Figure 5. We observe that there is a perfect correspondence between the numerical results and the theoretical error estimates predicted by Corollary 4.1.

Finally we fix a grid size $h = 0.25$, a time step $\Delta t = 0.1$ and make vary together the polynomial degrees, $N = r = 2, 3, 4, 5$. Figure 6 shows the decay of the error, that is again in agreement with (33).

5.2 Validation test

The second experiment is aimed at comparing the performance of our method with a DGSE space discretization coupled with leap-frog time integration scheme for the solution of (1).

We consider a plane wave propagating along the vertical direction in a (horizontally stratified) heterogeneous domain having dimensions $\Omega = (0, 100) \text{ m} \times (0, 100) \text{ m} \times (-1850, 0) \text{ m}$, cf. Figure 7 and Table 1. The source plane wave is polarized in the x direction and its time dependency is given by a unit amplitude Ricker wave with peak frequency at 2 Hz . The subdomains are discretized in space with a cartesian hexahedral grid having size h ranging from 15 m in the top layer to 50 m in the bottom layer. We impose a free surface condition

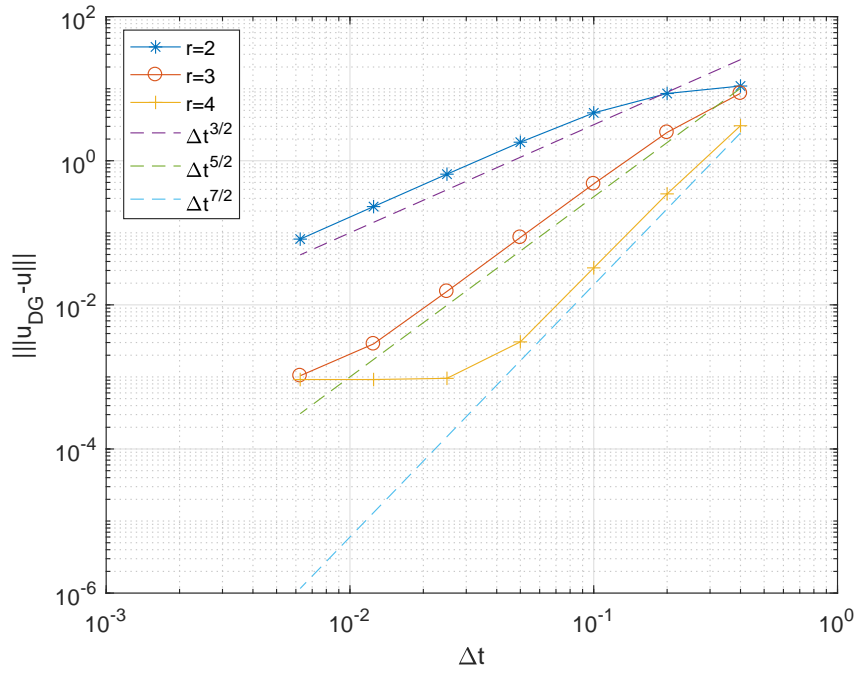


Figure 4: Computed errors $|||e||| = |||\mathbf{u}_{DG} - \mathbf{u}|||$ as a function of time-step Δt , with $r = 2, 3, 4$, $h = 0.125$ and $N = 4$.

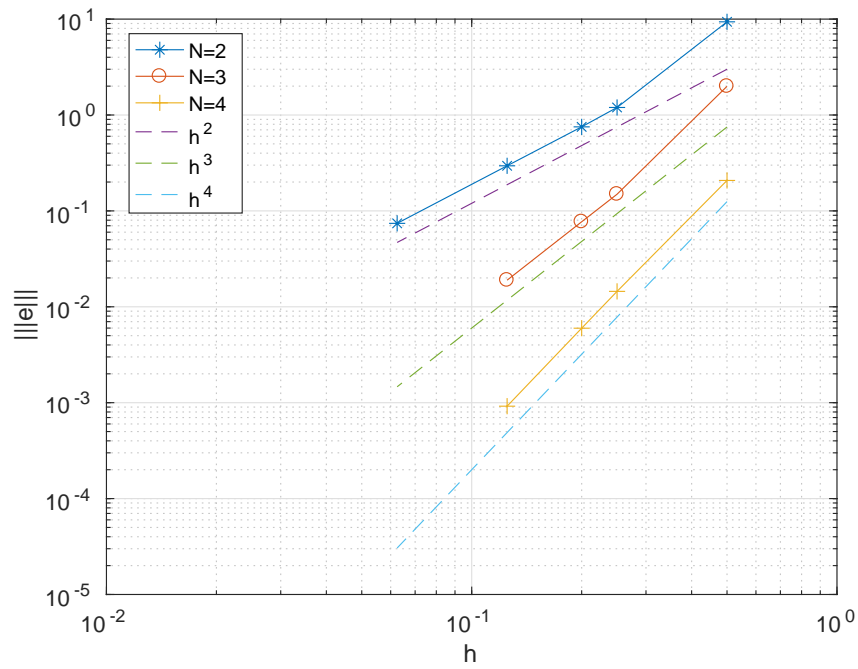


Figure 5: Computed errors $|||e||| = |||\mathbf{u}_{DG} - \mathbf{u}|||$ as a function of mesh size h , with $N = 2, 3, 4$, $\Delta t = 0.001$ and $r = 5$.

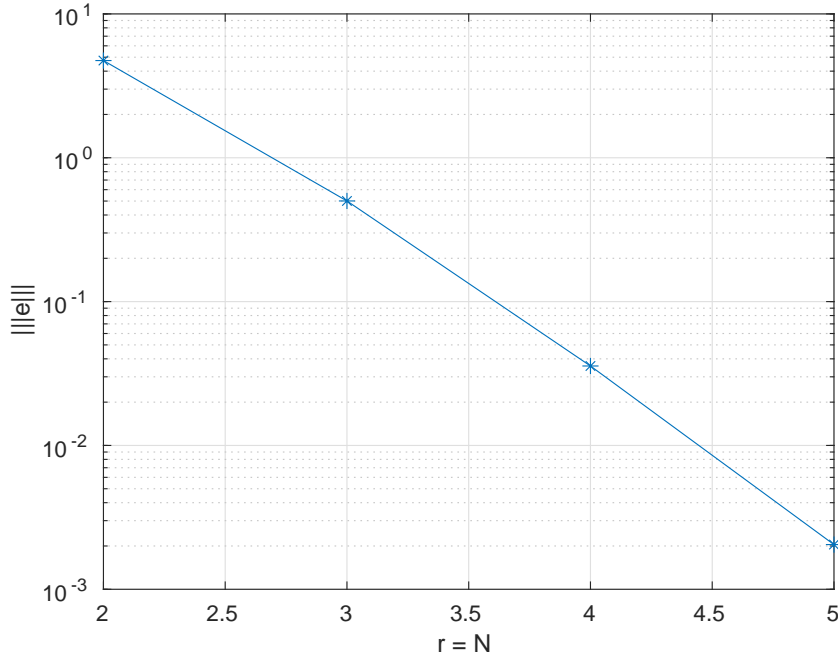


Figure 6: Computed errors $|||e||| = |||\mathbf{u}_{DG} - \mathbf{u}|||$ as a function of polynomial degree $N = r$, with $\Delta t = 0.1$, $h = 0.25$.

on the top surface, absorbing boundary conditions on the bottom surface and homogeneous Dirichlet conditions along the y and z direction on the remaining boundaries.

In Figure 8 (left) we report the computed time history of the first component of the displacement field, namely \mathbf{u}_x , on a receiver located at $(50\text{ m}, 50\text{ m}, 0\text{ m})$ on the free surface. We compare the results obtained with the space-time dG method (with $N_\ell = N = 2 \forall \ell$, $r_n = r = 2 \forall n$ and $\Delta t = 10^{-2}\text{ s}$) and the DGSE method coupled with the leap-frog scheme (with $N = 2$ and $\Delta t = 10^{-4}$) with a reference semi-analytical solution \mathbf{u}_{TH} obtained with the Thomson-Haskell propagation matrix method, [25]. As one can see the three different curves overlap each others and are in a good qualitative agreement. To have a quantitative measure of the misfits with respect to the semi analytical solution we report in Figure 8 (right) the time evolution of the error $e_x = |\mathbf{u}_{DG,x} - \mathbf{u}_{TH,x}|$. We notice that both numerical methods achieve the same level of accuracy. Finally, in Table 2, we compare the efficiency of the schemes here denoted as “time to solution”. From the second row in Table 2 we can conclude that the space-time dG scheme is as good as the leap-frog time integration. However, due to the assembly phase of the linear system in (30) it becomes much more expensive (third row in Table 2). In addition, if one employs a direct solver, this reveals to be a great limitation concerning the dimension of the problems that we can consider due to the amount of memory required to store the entries of the matrix. In this situation, a suitable iterative algorithm is preferable. This will be a topic for a future research.

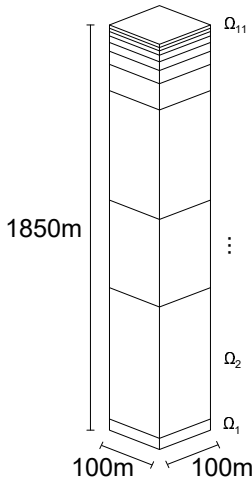


Figure 7: Computational domain $\Omega = \cup_{\ell=1}^{11} \Omega_\ell$

Layer	Height [m]	$\rho[kg/m^3]$	$c_p[m/s]$	$c_s[m/s]$	$\zeta[1/s]$
Ω_1	15	1800	1064	236	0.261
Ω_2	15	1800	1321	294	0.216
Ω_3	20	1800	1494	332	0.190
Ω_4	30	1800	1664	370	0.169
Ω_5	40	1800	1838	408	0.153
Ω_6	60	1800	2024	450	0.139
Ω_7	120	2050	1988	523	0.120
Ω_8	500	2050	1920	600	0.105
Ω_9	400	2400	3030	1515	0.041
Ω_{10}	600	2400	4180	2090	0.030
Ω_{11}	50	2450	5100	2850	0.020

Table 1: Mechanical properties for the considered test. Here, the Lamé parameters λ and μ can be obtained through the relations $\mu = \rho c_s^2$ and $\lambda = \rho c_p^2 - \mu$.

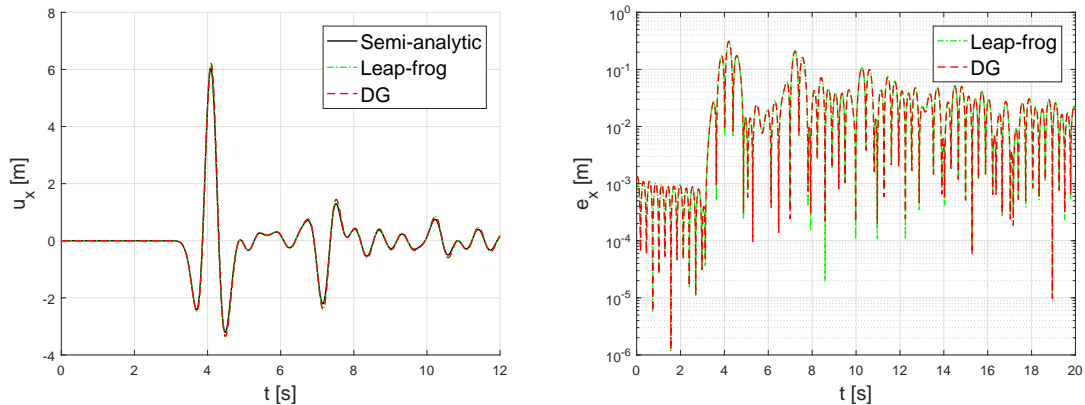


Figure 8: Left: time evolution of the first component of the displacement field \mathbf{u}_x at $(50\text{ m}, 50\text{ m}, 0\text{ m})$ computed with the DGSE method coupled with leap-frog scheme ($N = 2$, $\Delta t = 10^{-4}$) and the proposed space-time dG method ($N = r = 2$ and $\Delta t = 10^{-2}s$). The results are compared with a reference semi-analytical solution obtained with the Thomson-Haskell propagation matrix method, [25]. Right: the time evolution of the error $e_x = |\mathbf{u}_{DG,x} - \mathbf{u}_{TH,x}|$.

$N = r$	Leap-frog			Time-DG				
	Δt	Exec. time	error	Δt	nnz(A)	Mat. build	Time loop	error
2	10^{-4}	180s	0.065	10^{-1}	$8.6 \cdot 10^8$	39s	31s	0.104
2	10^{-4}	180s	0.065	10^{-2}	$8.6 \cdot 10^8$	39s	171s	0.065

Table 2: Comparison of the performance for the resolution of plane wave case test. Total execution time of the DGSE method coupled with the leap-frog scheme versus the space-time dG method. The accuracy of the methods is compared using the ℓ^2 -norm of the error in the x component of the displacement \mathbf{u}_x , computed using the semi-analytic solution

6 Conclusions

In this work we have presented a space-time Discontinuous Galerkin method for the numerical approximation of visco-elastic wave propagation problems. We have built an energy norm that naturally arose by the variational formulation of the problem, and that we have employed to prove well-posedness, stability and error bounds. We have implemented our method in the open-source software SPEED and we have verified and validated the proposed numerical algorithm on some three dimensional benchmarks.

7 Acknowledgements

Paola F. Antonietti and Ilario Mazzieri have been partially supported by the SIR Research Grant no. RBSI14VTOS funded by MIUR - Italian Ministry of Education, Universities and Research. This work was partially supported by "National Group of Computing Science" (GNCS-INdAM).

References

- [1] D. S. Abdi and F. X. Giraldo. Efficient construction of unified continuous and discontinuous Galerkin formulations for the 3d euler equations. *Journal of Computational Physics*, 320:46–68, 2016.
- [2] R. A. Adams and J. J. F. Fournier. *Sobolev spaces*, volume 140 of *Pure and Applied Mathematics*. Elsevier, Amsterdam, second edition, 2003.
- [3] S. Adjerid and H. Temimi. A discontinuous Galerkin method for the wave equation. *Computer Methods in Applied Mechanics and Engineering*, 200(5):837 – 849, 2011.
- [4] P. F. Antonietti, B. Ayuso de Dios, I. Mazzieri, and A. Quarteroni. Stability analysis of discontinuous Galerkin approximations to the elastodynamics problem. *Journal of Scientific Computing*, 68:143–170, 2016.
- [5] P. F. Antonietti, F. Bonaldi, and I. Mazzieri. A high-order discontinuous Galerkin approach to the elasto-acoustic problem. *Computer Methods in Applied Mechanics and Engineering*, 358, 2020.
- [6] P. F. Antonietti, A. Cangiani, J. Collis, Z. Dong, E. Georgoulis, S. Giani, and P. Houston. Review of discontinuous Galerkin finite element methods for partial differential equations on complicated domains. *Lecture Notes in Computational Science and Engineering*, 114:279–308, 2016.
- [7] P. F. Antonietti, N. Dal Santo, I. Mazzieri, and A. Quarteroni. A high-order discontinuous Galerkin approximation to ordinary differential equations with applications to elastodynamics. *IMA Journal of Numerical Analysis*, 38(4):1709–1734, 2018.
- [8] P. F. Antonietti, A. Ferroni, I. Mazzieri, R. Paolucci, A. Quarteroni, C. Smerzini, and M. Stupazzini. Numerical modeling of seismic waves by discontinuous spectral element methods. *ESAIM: Proceedings and Surveys*, 61:1–37, 2018.

- [9] P. F. Antonietti, A. Ferroni, I. Mazzieri, and A. Quarteroni. Dispersion-dissipation analysis of 3D continuous and discontinuous spectral element methods for the elastodynamics equation. *Geophysics Journal International*, 211(3):1554–1574, 2017.
- [10] P. F. Antonietti and I. Mazzieri. High-order discontinuous Galerkin methods for the elastodynamics equation on polygonal and polyhedral meshes. *Computer Methods in Applied Mechanics and Engineering*, 342:414 – 437, 2018.
- [11] P. F. Antonietti, I. Mazzieri, A. Quarteroni, and F. Rapetti. Non-conforming high order approximations of the elastodynamics equation. *Computer Methods in Applied Mechanics and Engineering*, 209:212–238, 2012.
- [12] C. Bajer. Triangular and tetrahedral space-time finite elements in vibration analysis. *International Journal for Numerical Methods in Engineering*, 23:2031–2048, 1986.
- [13] M. Behr. Simplex space–time meshes in finite element simulations. *International Journal for Numerical Methods in Fluids*, 57:1421–1434, 2008.
- [14] S. C. Brenner. Korn’s inequalities for piecewise H^1 vector fields. *Mathematics of Computation*, 73(247):1067–1087, 2004.
- [15] A. Cangiani, Z. Dong, E. H. Georgoulis, and P. Houston. hp -version discontinuous Galerkin methods for advection-diffusion-reaction problems on polytopic meshes. *ESAIM Mathematical Modelling and Numerical Analysis*, 50:699 – 725, 2016.
- [16] A. Cangiani, E. H. Georgoulis, and P. Houston. hp -version discontinuous Galerkin methods on polygonal and polyhedral meshes. *Mathematical Models and Methods in Applied Sciences*, 24(10):2009–2041, 2014.
- [17] C. Canuto, M. Y. Hussaini, A. Quarteroni, and T. A. Zang. *Spectral methods: Fundamentals in Single Domains*. Springer, Berlin, 2006.
- [18] C. Canuto, M. Y. Hussaini, A. Quarteroni, and T. A. Zang. *Spectral Methods: Evolution to Complex Geometries and Applications to Fluid Dynamics*. 2007.
- [19] M. Delfour, W. Hager, and F. Trochu. Discontinuous Galerkin methods for ordinary differential equations. *Mathematics of Computation*, 36(154):455–473, 1981.
- [20] J. Erickson, D. Guoy, J. Sullivan, and A. Üngör. Building space-time meshes over arbitrary spatial domains. *Engineering with Computers*, 20:342–353, 2005.
- [21] D. A. French. A space-time finite element method for the wave equation. *Computer Methods in Applied Mechanics and Engineering*, 107(1):145 – 157, 1993.
- [22] D. A. French and T. E. Peterson. A continuous space-time finite element method for the wave equation. *Mathematics of Computation*, 65:491–506, 1996.
- [23] E. H. Georgoulis, E. Hall, and P. Houston. Discontinuous Galerkin methods for advection-diffusion-reaction problems on anisotropically refined meshes. *SIAM Journal on Scientific Computing*, 30(1):246–271, 2007/08.

- [24] R. Griesmaier and P. Monk. Discretization of the wave equation using continuous elements in time and a hybridizable discontinuous Galerkin method in space. *Journal of Scientific Computing*, 58(2):472–498, 2014.
- [25] N. A. Haskell. The dispersion of surface waves on multilayered media. *Bulletin of the Seismological Society of America*, 43:17–43, 1953.
- [26] T. Hughes and G. Hulbert. Space-time finite element methods for elastodynamics: formulation and error estimates. *Computer Methods in Applied Mechanics and Engineering*, 66:339–363, 1988.
- [27] T. J. Hughes, L. P. Franca, and G. M. Hulbert. A new finite element formulation for computational fluid dynamics: Viii. the galerkin/least-squares method for advective-diffusive equations. *Computer Methods in Applied Mechanics and Engineering*, 73(2):173 – 189, 1989.
- [28] T. J. Hughes and G. M. Hulbert. Space-time finite element methods for second-order hyperbolic equations. *Computer Methods in Applied Mechanics and Engineering*, 84(3):327 – 348, 1990.
- [29] A. Idesman. Solution of linear elastodynamics problems with space–time finite elements on structured and unstructured meshes. *Computer Methods in Applied Mechanics and Engineering*, 196:1787–1815, 2007.
- [30] C. Johnson. Discontinuous Galerkin finite element methods for second order hyperbolic problems. *Computer Methods in Applied Mechanics and Engineering*, 107(1):117 – 129, 1993.
- [31] J. Kacur. Method of Rothe in evolution equations. In *Lecture Notes in Mathematics*, volume 1192, pages 23–34, 1970.
- [32] Z. Kamont. Numerical method of lines. In *Hyperbolic Functional Differential Inequalities and Applications*, pages 181–204. Springer Netherlands, 1999.
- [33] O. Karakashian and C. Makridakis. Convergence of a continuous Galerkin method with mesh modification for nonlinear wave equations. *Mathematics of Computation*, 74:85–102, 2005.
- [34] U. Köcher and M. Bause. Variational space–time methods for the wave equation. *Journal of Scientific Computing*, 61(2):424–453, 2014.
- [35] A. Kroopnick. Bounded and L^2 -solutions to a second order nonlinear differential equation with a square integrable forcing term. *International Journal of Mathematics and Mathematical Sciences*, 22(3):569–571, 1999.
- [36] I. Mazzieri, M. Stupazzini, R. Guidotti, and C. Smerzini. SPEED: Spectral Elements in Elastodynamics with Discontinuous Galerkin: a non-conforming approach for 3D multi-scale problems. *International Journal for Numerical Methods in Engineering*, 95(12):991–1010, 2013.

- [37] I. Perugia and D. Schötzau. An hp -analysis of the local discontinuous Galerkin method for diffusion problems. *Journal of Scientific Computing*, 17(1-4):561–571, 2002.
- [38] B. Rivière, S. Shaw, M. F. Wheeler, and J. R. Whiteman. Discontinuous Galerkin finite element methods for linear elasticity and quasistatic linear viscoelasticity. *Numerische Mathematik*, 95(2):347–376, 2003.
- [39] B. Rivière, S. Shaw, and J. Whiteman. Discontinuous Galerkin finite element methods for dynamic linear solid viscoelasticity problems. *Numerical Methods for Partial Differential Equations*, 23(5):1149–1166, 2007.
- [40] C. Schwab. *p - and hp - Finite Element Methods: Theory and Applications in Solid and Fluid mechanics*. Oxford University Press, 1998.
- [41] T. Tezduyar, S. Sathe, R. Keedy, and K. Stein. Space–time finite element techniques for computation of fluid–structure interactions. *Computer Methods in Applied Mechanics and Engineering*, 195:2002–2027, 2006.
- [42] L. L. Thompson and P. M. Pinsky. A space-time finite element method for structural acoustics in infinite domains part 1: Formulation, stability and convergence. *Computer Methods in Applied Mechanics and Engineering*, 132(3):195 – 227, 1996.
- [43] A. Üngör and A. Sheffer. Tent-pitcher: A meshing algorithm for space-time discontinuous Galerkin methods. *Proceeding 9th International Meshing Roundtable*, 196:111–122, 2000.
- [44] N. J. Walkington. Combined DG–CG time stepping for wave equations. *SIAM Journal on Numerical Analysis*, 52:1398–1417, 2014.
- [45] Y. Yang, S. Chirputkar, D. N. Alpert, T. Eason, S. Spottswood, and D. Qian. Enriched space–time finite element method: a new paradigm for multiscaling from elastodynamics to molecular dynamics. *International Journal for Numerical Methods in Engineering*, 92(2):115–140, 2012.

MOX Technical Reports, last issues

Dipartimento di Matematica
Politecnico di Milano, Via Bonardi 9 - 20133 Milano (Italy)

- 41/2019** Abbà, A.; Bonaventura, L.; Recanati, A.; Tugnoli, M.;
Dynamical p -adaptivity for LES of compressible flows in a high order DG framework
- 42/2019** Martino, A.; Guatteri, G.; Paganoni, A.M.
hmmhdd Package: Hidden Markov Model for High Dimensional Data
- 39/2019** Lovato, I.; Pini, A.; Stamm, A.; Taquet, M.; Vantini, S.
Multiscale null hypothesis testing for network-valued data: analysis of brain networks of patients with autism
- 40/2019** Lovato, I.; Pini, A.; Stamm, A.; Vantini, S.
Model-free two-sample test for network-valued data
- 38/2019** Massi, M.C.; Ieva, F.; Gasperoni, F.; Paganoni, A.M.
Minority Class Feature Selection through Semi-Supervised Deep Sparse Autoencoders
- 37/2019** Menafoglio, A.; Secchi, P.
O2S2: a new venue for computational geostatistics
- 36/2019** Salvador, M.; Dede', L.; Quarteroni, A.
An intergrid transfer operator using radial basis functions with application to cardiac electromechanics
- 33/2019** Regazzoni, F.; Dede', L.; Quarteroni, A.
Machine learning of multiscale active force generation models for the efficient simulation of cardiac electromechanics
- 34/2019** Antonietti, P. F.; Mazzieri, I.; Melas, L.; Paolucci, R.; Quarteroni, A.; Smerzini, C.; Stupazzini, C.
Three-dimensional physics-based earthquake ground motion simulations for seismic risk assessment in densely populated urban areas
- 35/2019** Zancanaro, M.; Ballarin, F.; Perotto, S.; Rozza, G.
Hierarchical model reduction techniques for flow modeling in a parametrized setting